Supplementary information

Synthesis and electronic properties of nitrogen-doped π-extended polycyclic aromatic dicarboximides with multiple redox processes

Matías J. Alonso-Navarro[a,c†], Alexandra Harbuzaru[b†], Marcos Martínez[a], Paula Pérez Camero,[b] J. Teodomiro López Navarrete,[b] M. Mar Ramos,[c] Rocío Ponce Ortiz[b]*, José L. Segura [a]*

[a]*Department of Organic Chemistry, Complutense University of Madrid, Faculty of Chemistry, Madrid 28040, Spain.*
[b]*Department of Physical Chemistry, University of Málaga, Málaga, 29071, Spain.*
[c]*Chemical and Environmental Technology Department. Univ. Rey Juan Carlos, Móstoles, 28933, Spain.*

[†]These authors contributed equally to this work

Contents

1. General Information

All the chemicals were purchased from commercial suppliers and used without further purification. Compounds **1**,**2**,**3**,**4** were obtained as previously described.[1-3] ^{1}H-NMR and ^{13}C-NMR spectra were recorded on a Bruker Avance 300 MHz spectrometer. Chemical shifts are reported in ppm and referenced to the residual non-deuterated solvent frequencies ($CDCl_3$: δ 7.26 ppm for ^{1}H, δ 77.0 ppm for ^{13}C, $C_2D_2Cl_4$: δ 5.91 ppm for ^{1}H, δ 77.8 ppm for ^{13}C, TFA-d: δ 11.50 ppm for ^{1}H, δ 164.2 and 116.6 ppm for ^{13}C). Two-dimensional homonuclear (^{1}H-^{1}H) and heteronuclear (^{1}H-^{13}C) NMR correlation experiments were recorded on a Bruker AVIII 700 MHz spectrometer. UV–vis absorption spectra of the compounds in HPLC chloroform solutions at 20 ºC were recorded on a Varian Cary 50 UV–vis spectrophotometer. Mass spectra were recorded on a Bruker Reflex 2 (MALDI-TOF). FTIR spectra were carried out in a Shimadzu FTIR 8300 spectrophotometer. Cyclic voltammograms were recorded in an inert atmosphere in electrochemical workstation at a scan rate of 200 mV·s-1 at 20 ºC using tetrabutylammonium hexafluorophosphate (TBAHFP, 0.1 mol L^{-1}) as supporting electrolyte in dichloromethane. Polymer-precoated platinum electrode, platinum–wire electrode, and Ag/Ag^{+} electrode were used as working electrode, an auxiliary electrode, and reference electrode, respectively. Potentials were recorded versus Fc/Fc^{+}.

2. Synthesis of compounds and characterization

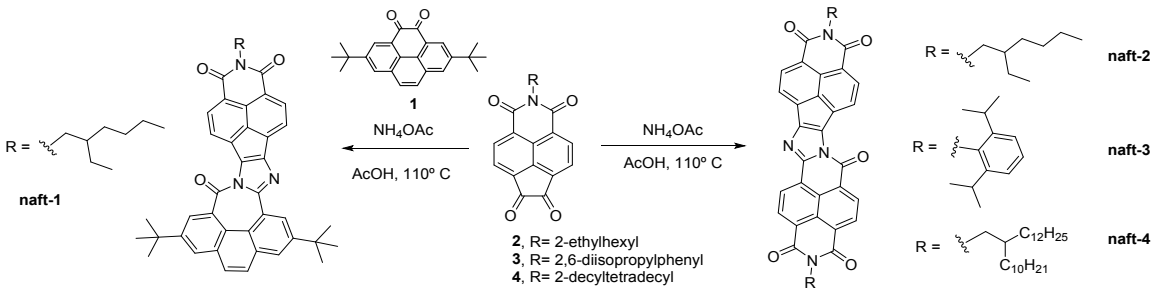

Scheme S1 Synthetic route for the novel compounds described in this article.

General Procedure for the synthesis of the cross-condensation compound:

An equimolar mixture of **1** and **2** and ammonium acetate (8 eq) were suspended in 10 mL of glacial acetic acid and the mixture was heated to 110 °C overnight under stirring. The reaction was cooled, and 40 mL of methanol were added. The dark precipitate was filtered and washed with distilled water, methanol, and hot methanol. The solid was purified by a chromatography column in dichloromethane.

naft-1: After the purification step, a green solid was obtained (20 mg, 20%).

^{1}H-NMR (300 MHz, $CDCl_3$/TFA-*d*): δ (ppm) = 9.95 (s, 1H), 9.23 (d, J = 7.5 Hz, 1H), 9.03 (d, J = 7.6 Hz, 1H), 8.91 (s, 1H), 8.84 (d, J = 7.6 Hz, 1H), 8.78 (d, J = 7.5 Hz, 1H), 8.48 (s, 1H), 8.43 (s, 1H), 8.13 (d, J = 8.9 Hz, 1H), 8.08 (d, J = 8.9 Hz, 1H), 4.28 (m , 2H), 1.99 (s, 1H), 1.78 (s, 9H), 1.67 (s, 9H), 1.53 – 1.40 (m, 8H), 0.96 – 0.85 (m, 6H).

^{13}C-NMR (75 MHz, $CDCl_3$): δ (ppm) = 162.52, 162.29, 157.19, 148.49, 147.96, 146.12, 138.64, 129.46, 129.18, 128.10, 127.28, 126.28, 125.46, 123.84, 123.54, 123.10, 122.70, 122.16, 121.65, 121.43, 119.88, 119.66, 119.23, 44.31, 38.55, 35.45, 35.13, 31.92, 30.86, 29.86, 28.71, 24.08, 23.48, 14.40, 10.65.

FTIR (ATR, $CHCl_3$): υ (cm^{-1}): 2961.62, 2923.48, 2866.55, 1719.56, 1701.75, 1359.40, 1266.08, 882.76, 761.76, 755.27.

MALDI-HRMS (m/z): calculated for $C_{46}H_{45}N_3O_3$: 687.3461, found (M^+): 687.3492.

General Procedure for the synthesis of the auto-condensation compounds:

The corresponding diketone **2**, **3** or **4** (1 eq) and ammonium acetate (8 eq) were suspended in 10 mL of glacial acetic acid and the mixture was heated to 110 °C overnight under stirring. The reaction was cooled, and 40 mL of methanol were added. The dark precipitate was filtered and washed with distilled water, methanol and hot methanol.

naft-2: a dark purple solid was obtained without further purification (40 mg, 84% yield).

^{1}H-NMR (300 MHz, $C_2D_2Cl_4$/TFA-*d*): δ (ppm) = 9.13 (d, J = 7.7 Hz, 1H), 8.93 (m , 2H), 8.87 (d, J = 7.7 Hz, 1H), 8.60 (d, J = 7.5 Hz, 1H), 8.55 (d, J = 7.5 Hz, 1H), 8.50 (d, J = 7.5 Hz, 1H), 8.18 (d, J = 7.5 Hz, 1H), 4.15 – 4.03 (m, 4H), 1.91 – 1.78 (m, 2H), 1.37 – 1.17 (m, 16H), 0.85 (m, 12H).

^{13}C-NMR (75 MHz, $C_2D_2Cl_4$/TFA-*d*): δ (ppm) = 168.77, 168.70, 167.37, 167.26, 160.75, 150.17, 147.94, 140.14, 138.66, 137.48, 137.15, 136.87, 136.11, 134.48, 133.82, 133.22, 132.96, 132.61, 131.82, 131.31, 130.00, 129.72, 128.75, 128.49, 127.97, 127.90, 124.57, 124.21, 49.47, 49.04, 42.12, 41.86, 34.50, 32.35, 27.81, 26.90, 17.81, 14.29.

FTIR (ATR, $CHCl_3$): υ (cm^{-1}): 2959.98, 2925.29, 2859.03, 1700.24, 1661.16, 1336.99, 1238.44, 767.30, 756.27.

MALDI-HRMS (m/z): calculated for $C_{44}H_{42}N_4O_5$: 706.3155, found (M^+): 706.3138.

naft-3: a purple solid was obtained without further purification (44 mg, 64% yield).

^{1}H-NMR (300 MHz, $CDCl_3$): δ (ppm) = 9.08 (d, J = 7.6 Hz, 1H), 8.95 (d, J = 7.6 Hz, 1H), 8.93 (m, J = 7.7 Hz, 1H), 8.89 (d, J = 7.7 Hz, 1H), 8.57 (m, 2H), 8.50 (d, J = 7.5 Hz, 1H), 8.20 (d, J = 7.5 Hz, 1H), 7.56 – 7.46 (m, 2H), 7.37 (d = 8.0 Hz, 2H), 7.34 (d = 8.0 Hz, 2H), 2.88 – 2.68 (m, 4H), 1.20 (s, 12H), 1.17 (s, 12H).

^{13}C-NMR (75 MHz, $CDCl_3$): δ (ppm) = 163.58, 162.99, 162.84, 158.39, 153.04, 149.05, 145.98, 145.70, 136.34, 134.31, 132.99, 132.82, 132.65, 132.55, 131.48, 131.34, 130.95, 130.82, 130.16, 130.09, 129.74, 128.84, 128.45, 126.57, 126.23, 126.11, 125.28, 124.40, 124.14, 123.98, 123.79, 123.66, 29.45, 29.30, 24.20, 24.18.

FTIR (ATR, $CHCl_3$): υ (cm^{-1}): 3067.03, 2963.19, 2928.27, 2870.23, 1712.78, 1674.95, 1639.61, 1341.29, 1459.81, 1341.37, 1241.48, 1174.41, 764.86, 7850.59, 726.34.

MALDI-HRMS (m/z): calculated for $C_{52}H_{42}N_4O_5$: 802.3155, found (M^+): 802.3192.

naft-4: After a chromatography column in $CHCl_3$/MeOH 100:1, a dark purple solid was obtained (58 mg, 60% yield).

^{1}H-NMR (300 MHz, $CDCl_3$): δ (ppm) = 8.81 (d, J = 7.6 Hz, 1H), 8.71 (d, J = 7.6 Hz, 1H), 8.66 (s, 2H), 8.33 (d, J = 7.5 Hz, 1H), 8.25 (d, J = 7.5 Hz, 1H), 8.21 (d, J = 7.6 Hz, 1H), 7.90 (d, J = 7.6 Hz, 1H), 4.12 (d, J = 7.2 Hz, 2H), 4.03 (d, J = 7.2 Hz, 2H), 1.27 (m, 78H), 0.95 – 0.80 (m, 12H).

^{13}C-NMR (75 MHz, $CDCl_3$): δ (ppm) = 163.27, 163.14, 162.76, 162.58, 157.45, 152.33, 148.42, 135.42, 133.12, 132.10, 132.02, 131.73, 131.31, 130.37, 128.50, 127.25, 125.69, 125.32, 125.10, 125.00, 124.33, 124.24, 123.82, 123.45, 123.40, 123.22, 45.12, 44.56, 37.10, 36.88, 32.09, 31.82, 30.27, 29.89, 29.85, 29.54, 26.68, 26.62, 22.85, 14.27.

FTIR (ATR, $CHCl_3$): υ (cm^{-1}): 2955.11, 2923.45, 2853.46, 1704.57, 1666.28, 1464.74, 1402.09, 765.67, 757.74.

MALDI-HRMS (m/z): calculated for $C_{76}H_{106}N_4O_5$: 1154.8163, found (M^+): 1154.8209.

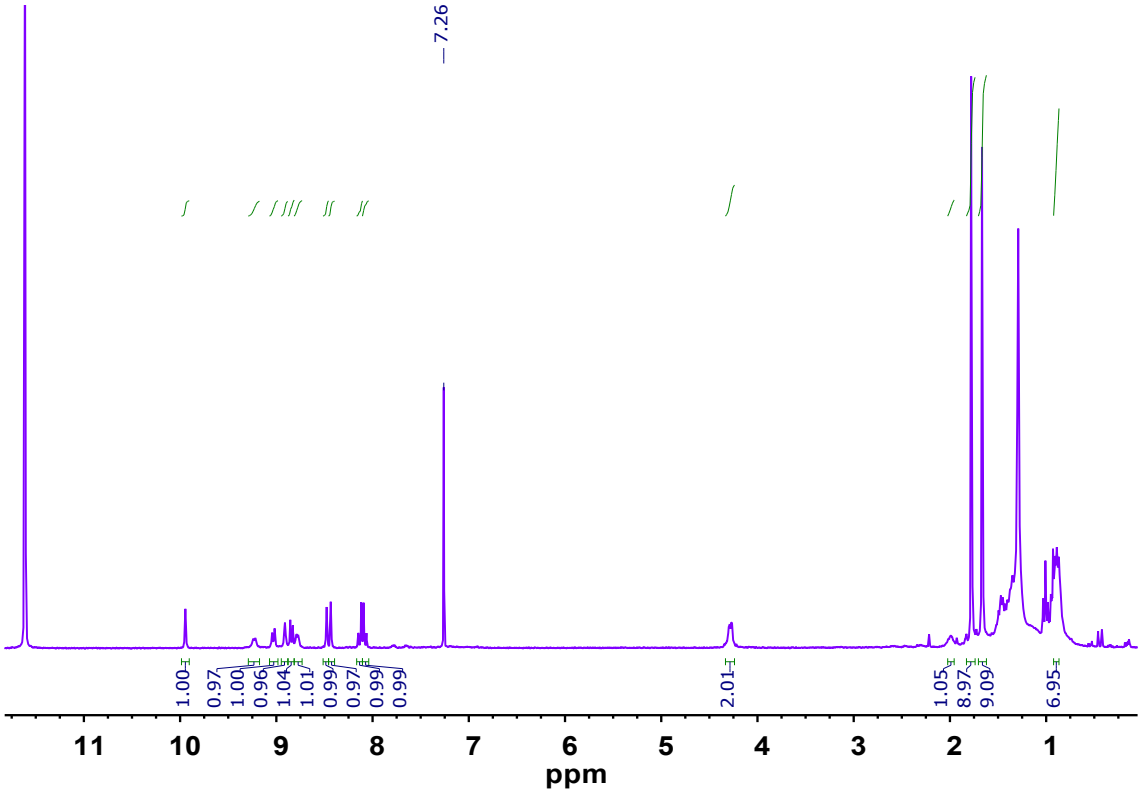

Figure S1 ^{1}H-NMR spectrum of **naft-1** in $CDCl_3$/TFA-*d*.

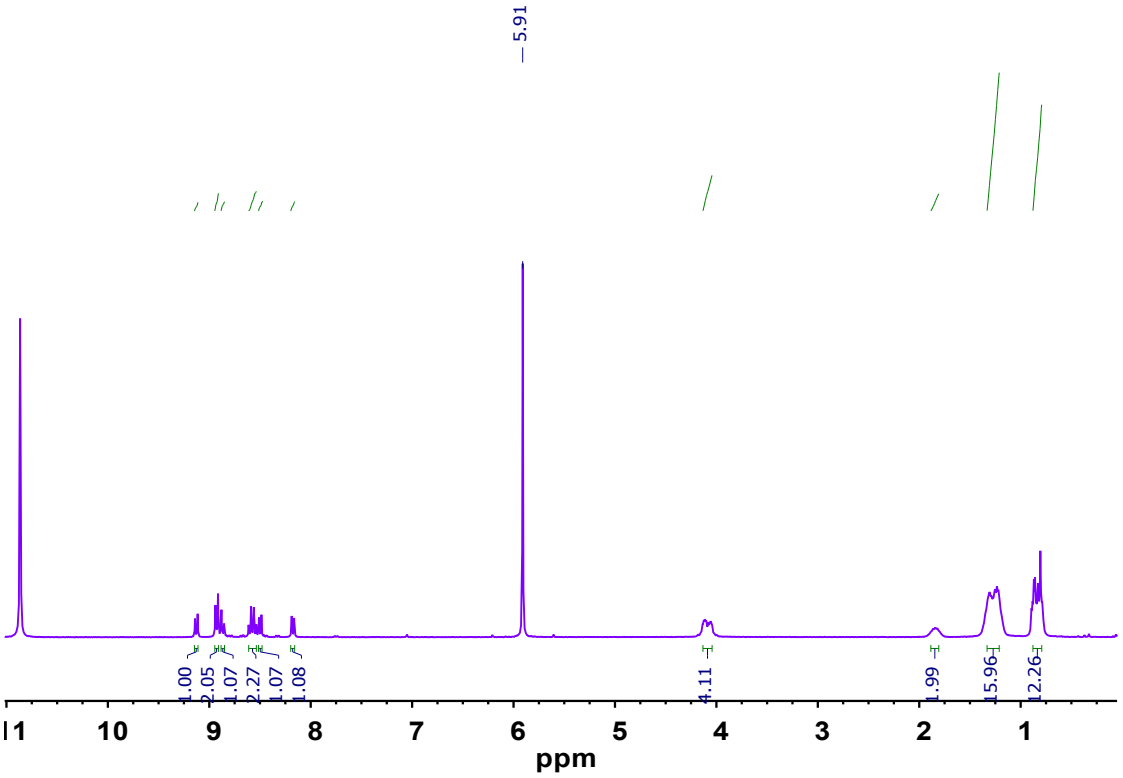

Figure S2 ^{1}H-NMR spectrum of **naft-2** in $C_2D_2Cl_4$/TFA-*d*.

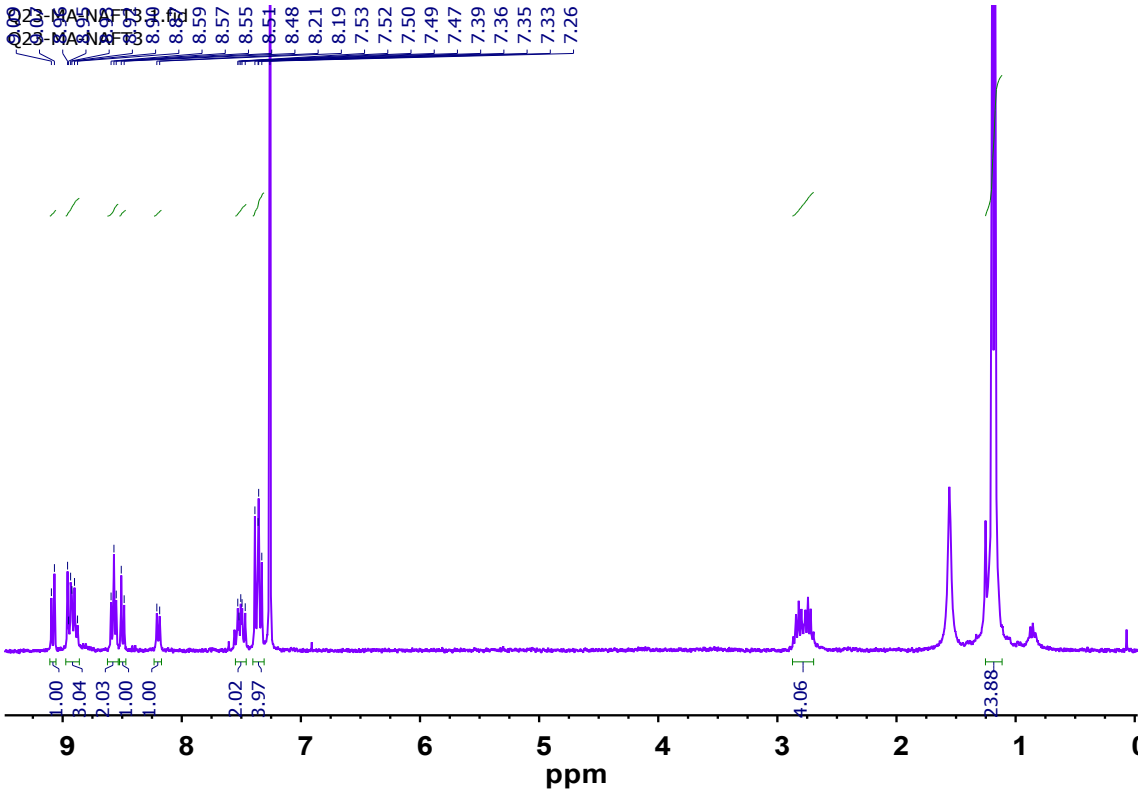

Figure S3 ^{1}H-NMR spectrum of **naft-3** in $CDCl_3$.

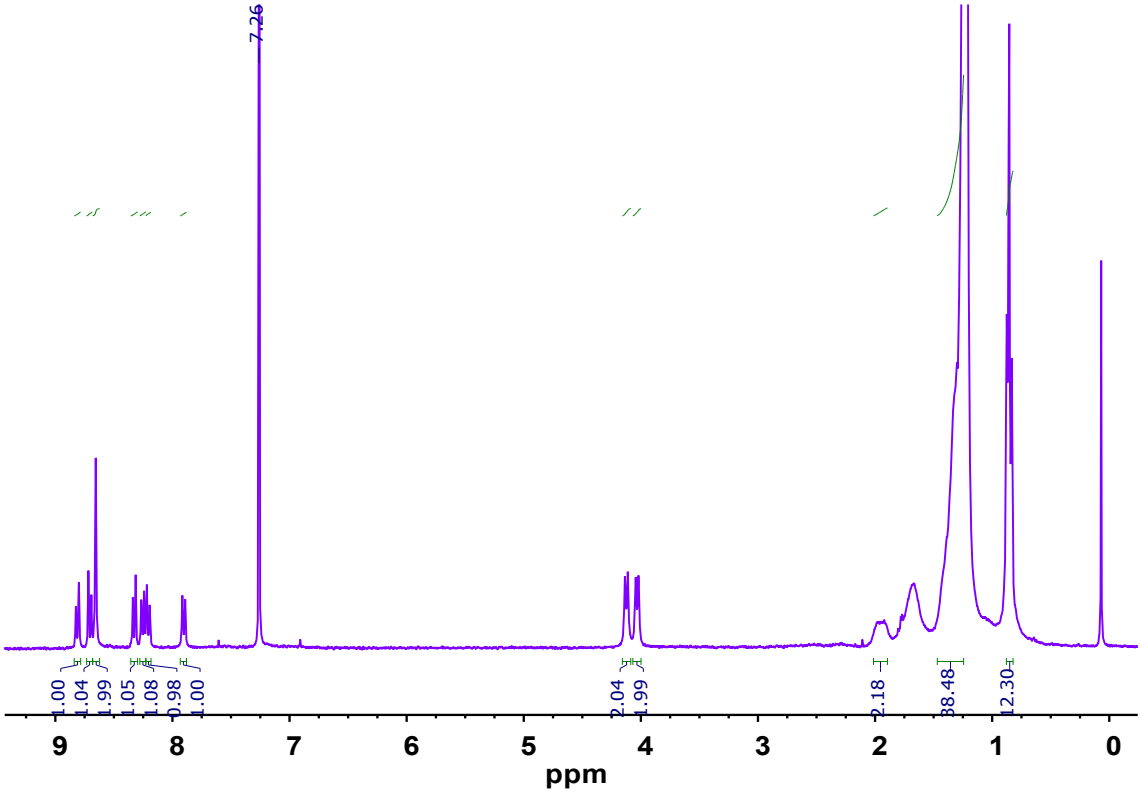

Figure S4 ^{1}H-NMR spectrum of **naft-4** in $CDCl_3$.

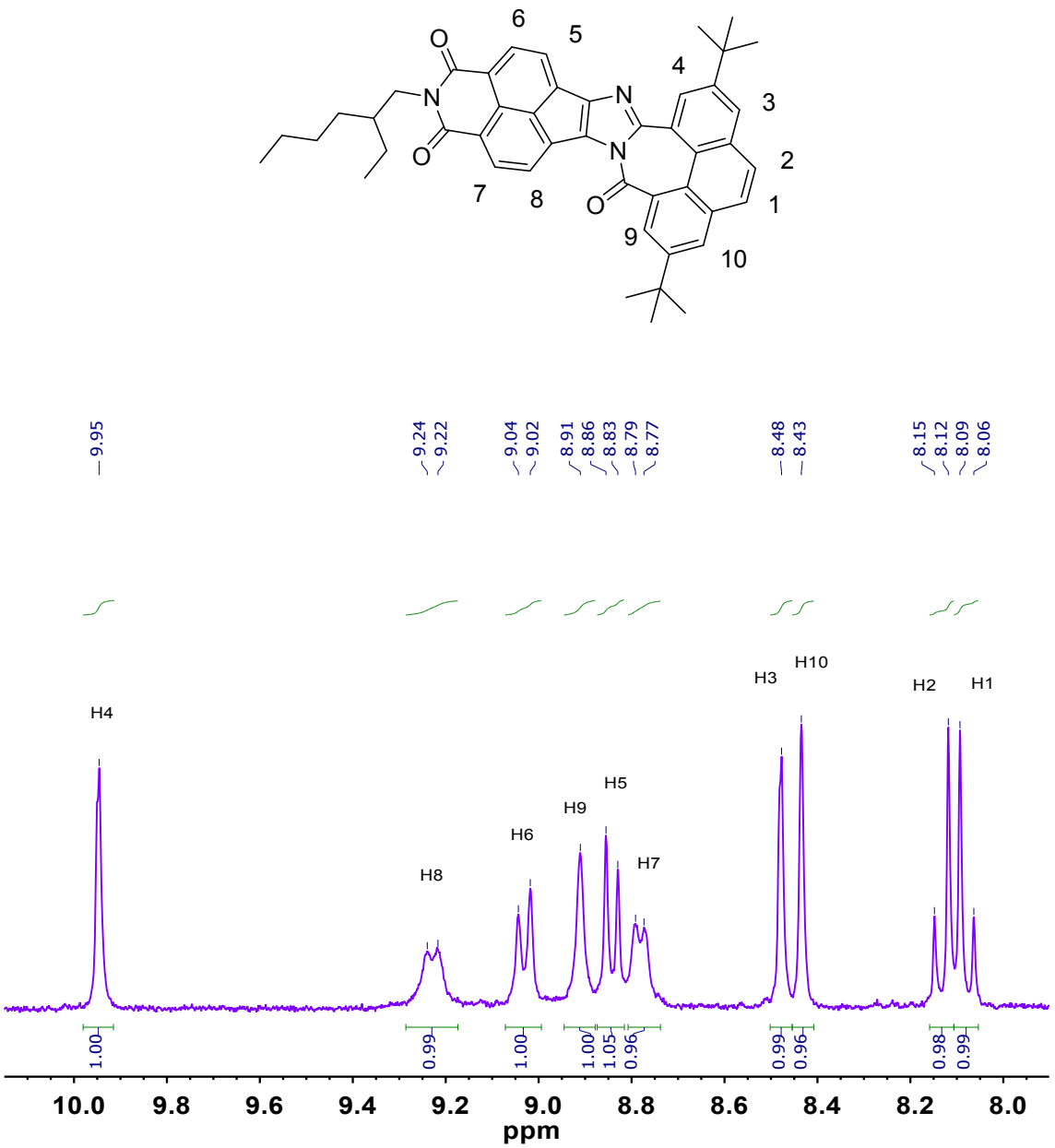

Figure S5 ^{1}H-NMR spectra of **naft-1** in $CDCl_3$/TFA-*d*.

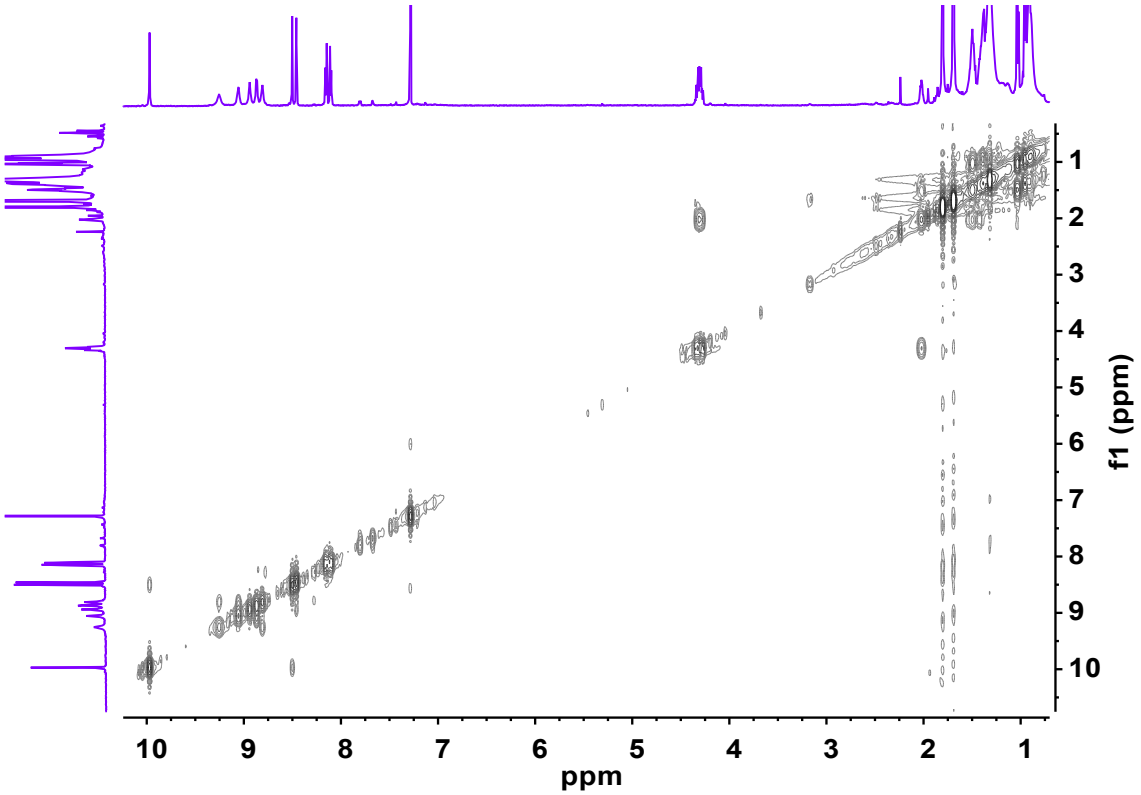

Figure S6 COSY ^{1}H-^{1}H NMR spectra of **naft-1** in $CDCl_3$/TFA-*d*.

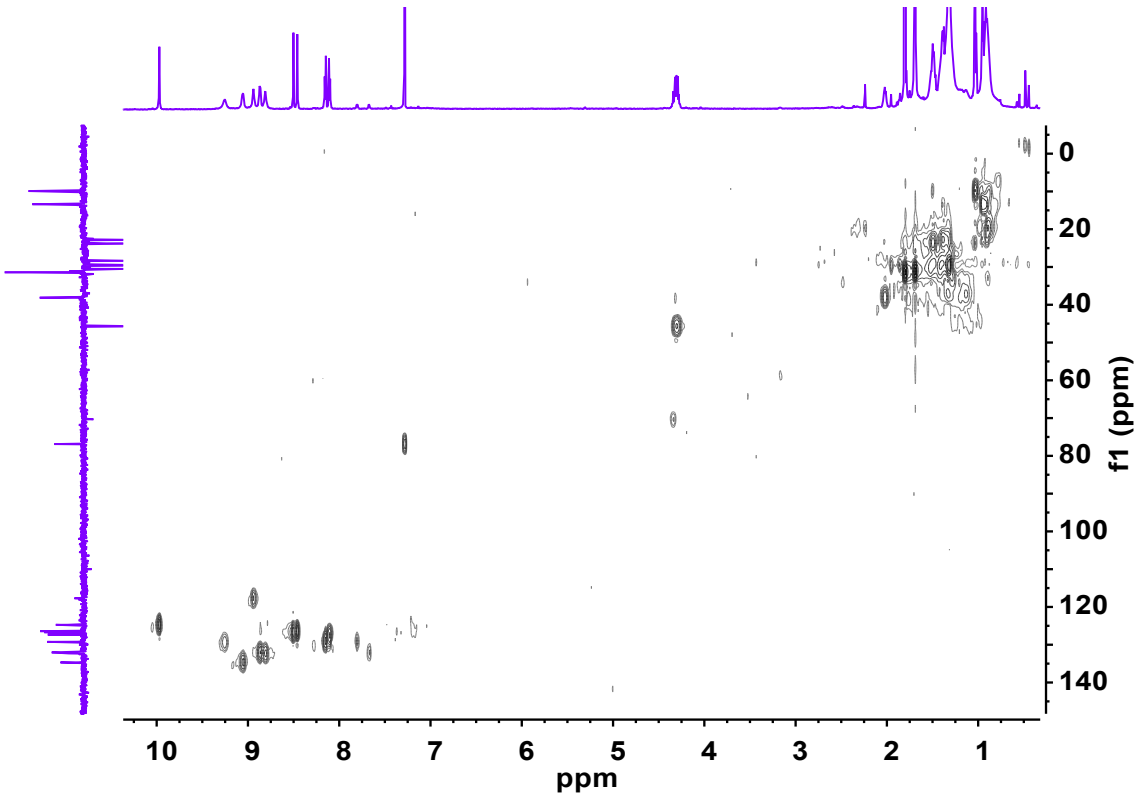

Figure S7 HSQC ^{1}H-^{13}C NMR spectra of **naft-1** in $CDCl_3$/TFA-*d*.

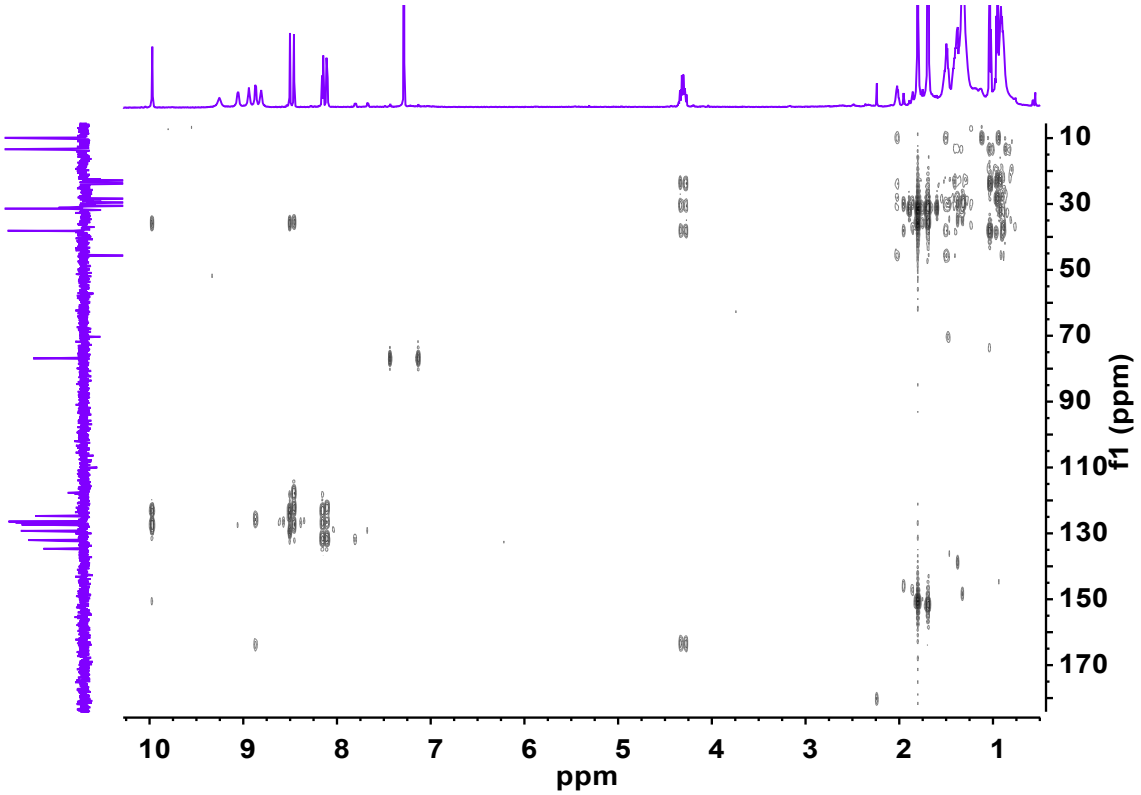

Figure S8 HMBC ^{1}H-^{13}C NMR spectra of **naft-1** in $CDCl_3$/TFA-*d*.

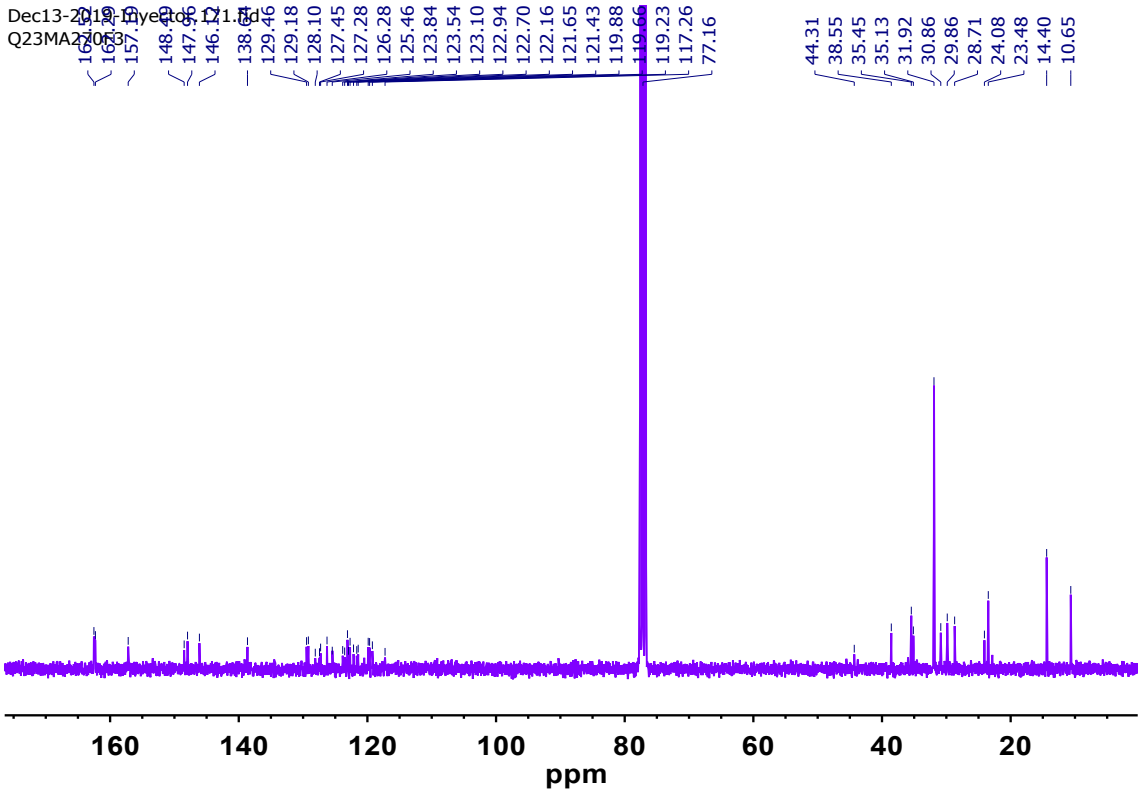

Figure S9 ^{13}C-NMR spectrum of ***naft-1*** in $CDCl_3$.

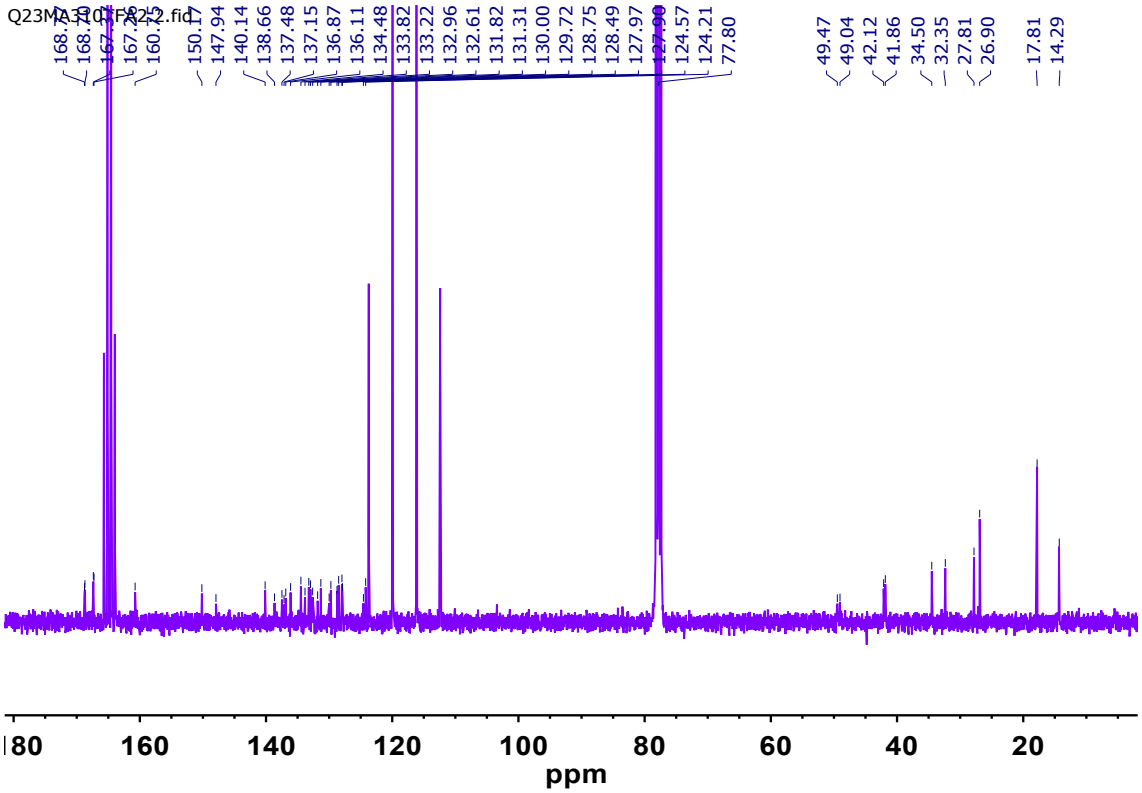

Figure S10 ^{13}C-NMR spectrum of **naft-2** in $CDCl_3$/TFA-d.

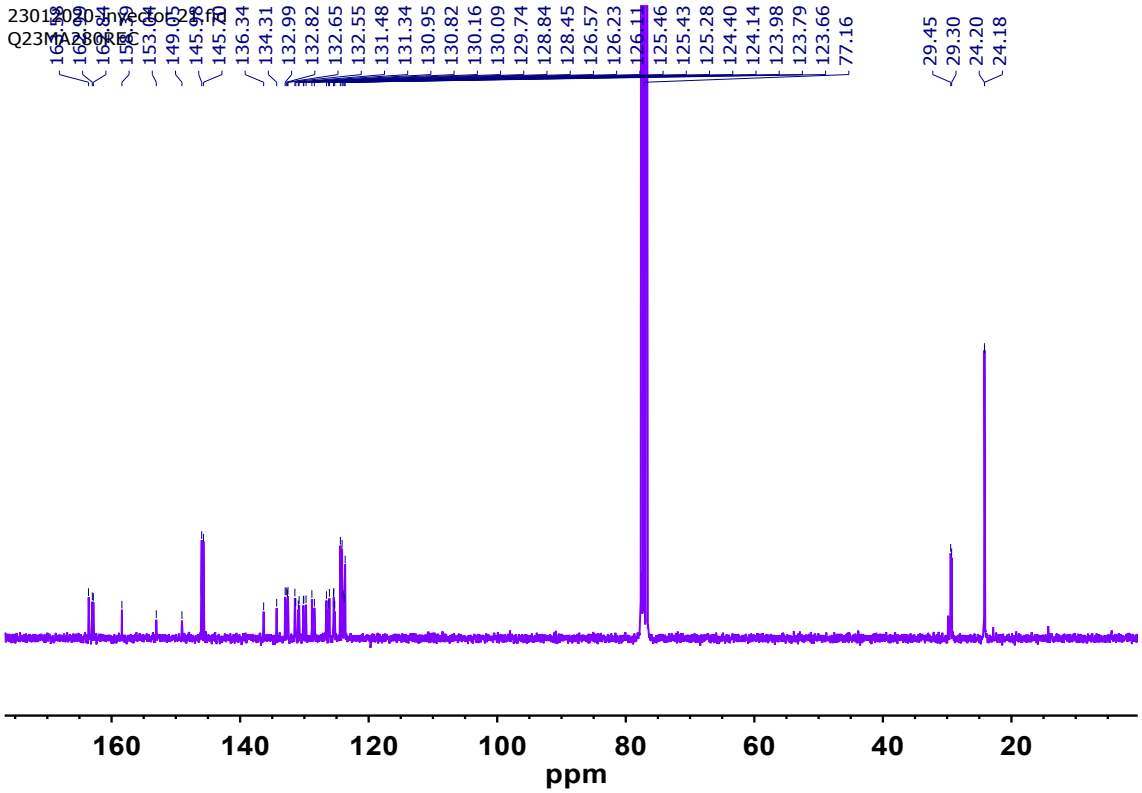

Figure S11 ^{13}C-NMR spectrum of **naft-3** in $CDCl_3$.

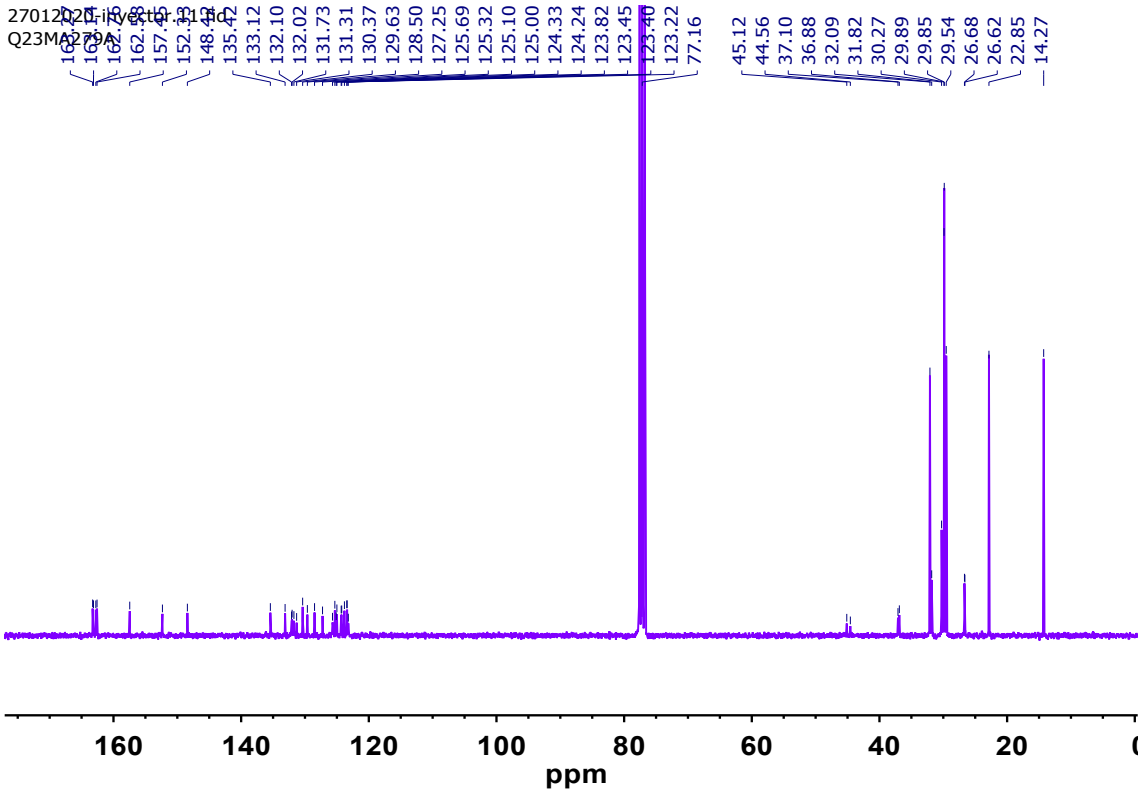

Figure S12 ^{13}C-NMR spectrum of **naft-4** in $CDCl_3$.

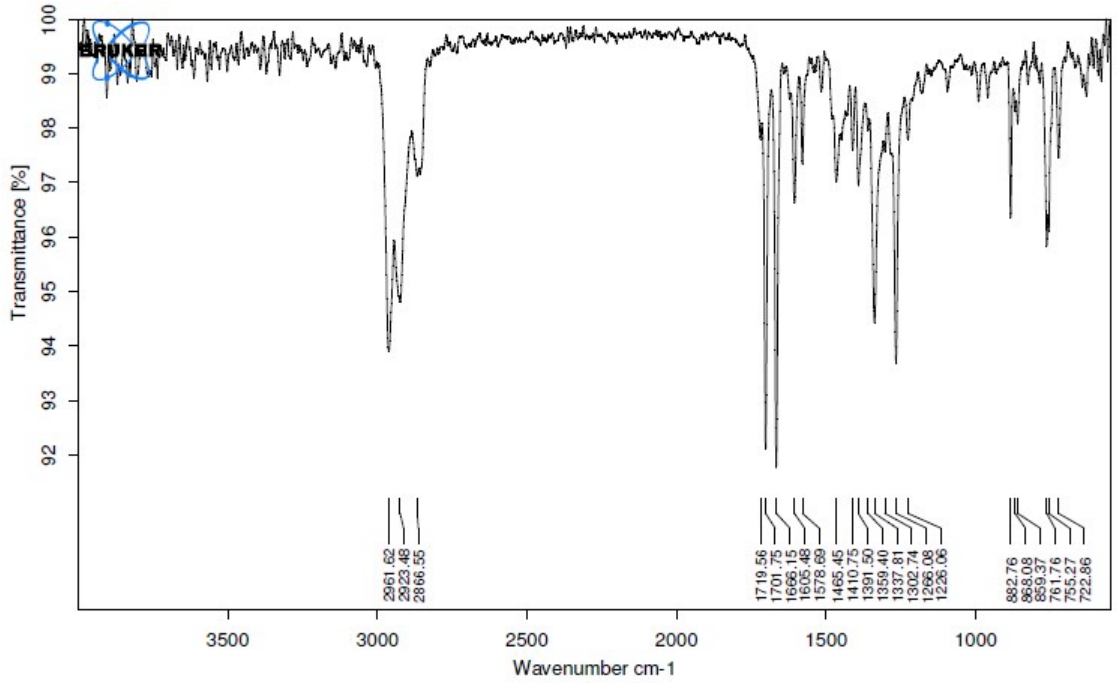

Figure S13 IR spectrum of **naft-1**.

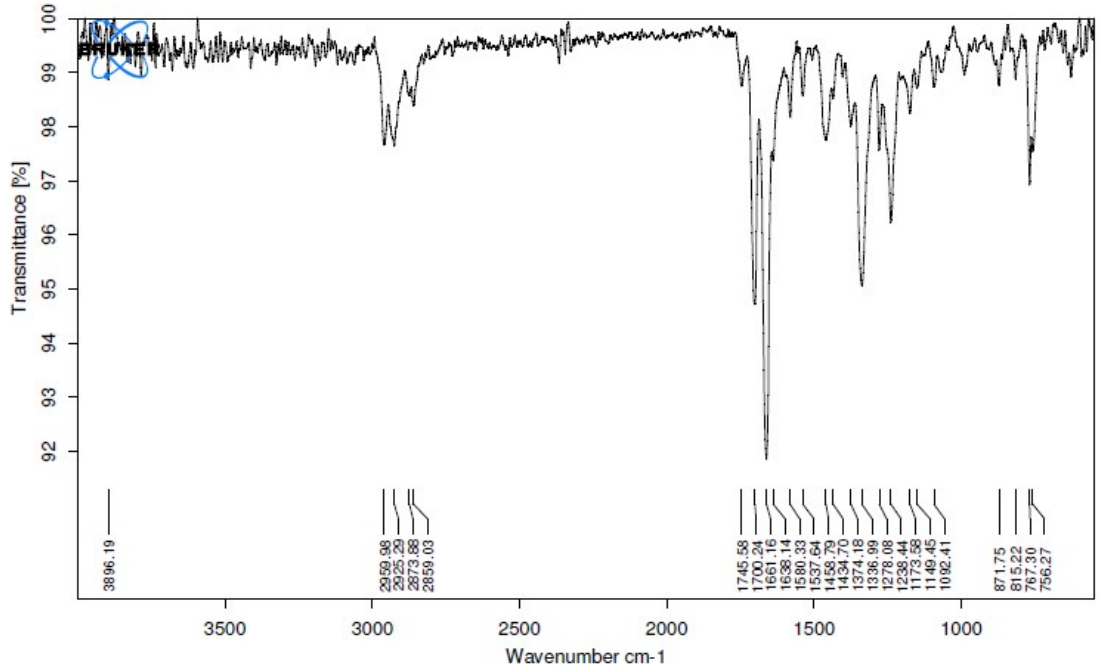

Figure S14 IR spectrum of **naft-2**.

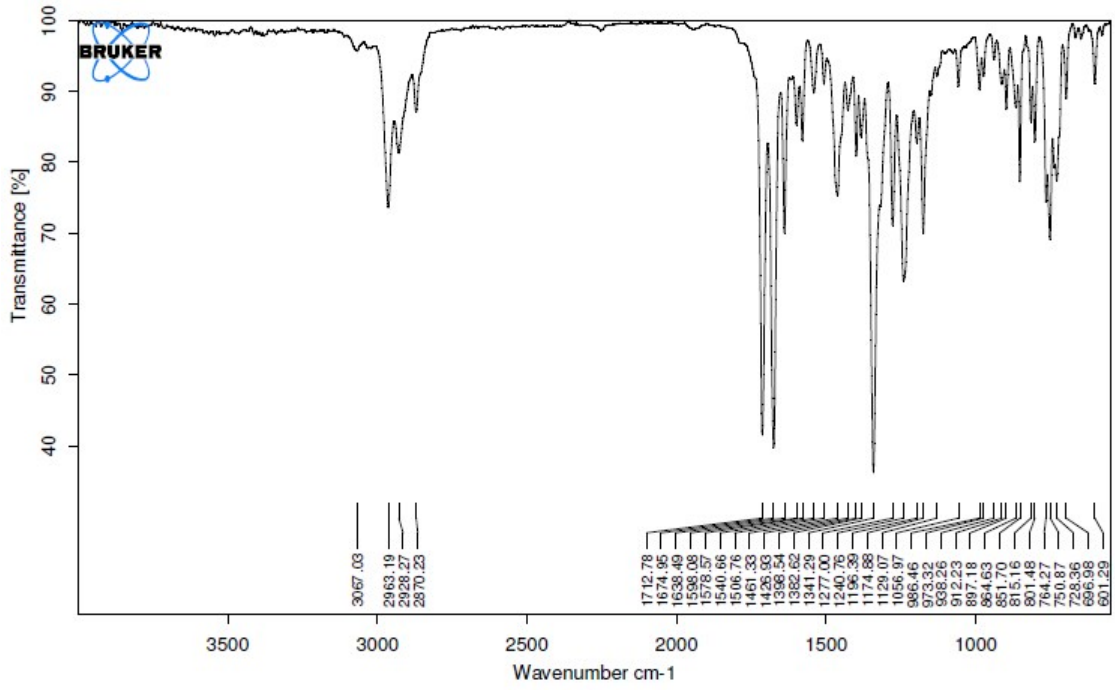

Figure S15 IR spectrum of **naft-3**.

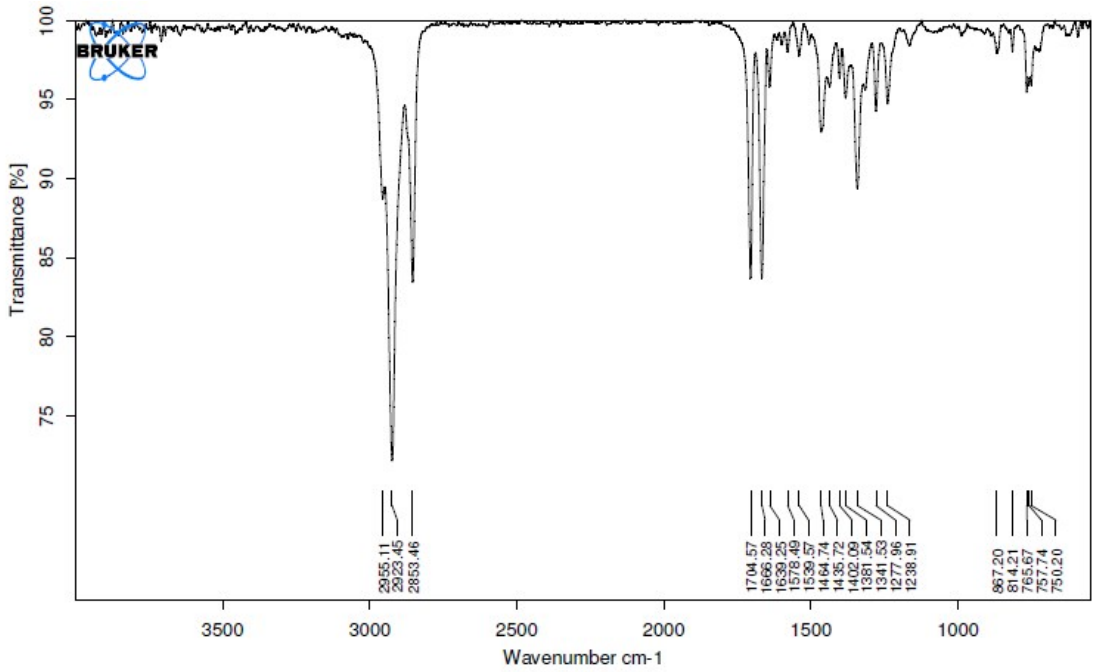

Figure S16 IR spectrum of **naft-4**.

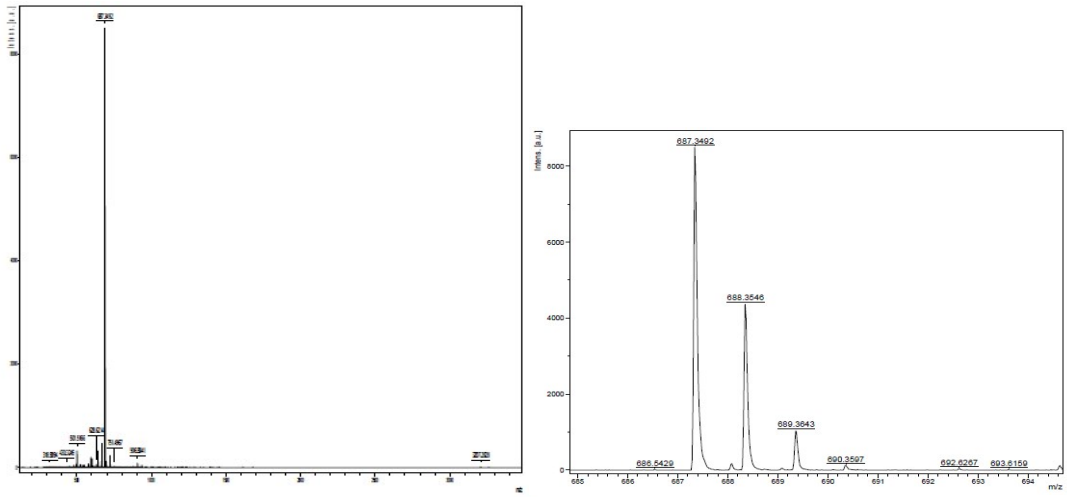

Figure S17 MALDI-HRMS (m/z) spectrum of **naft-1**.

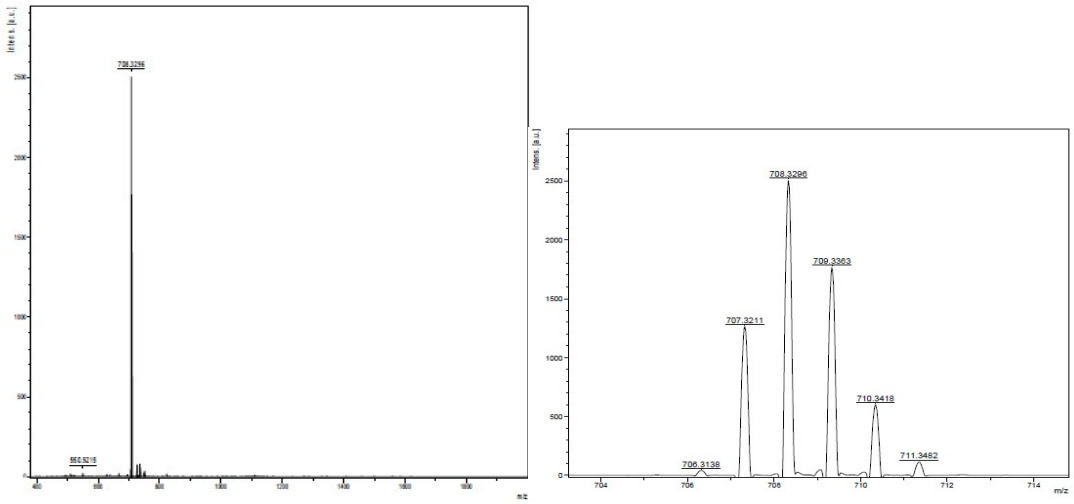

Figure S18 MALDI-HRMS (m/z) spectrum of **naft-2**.

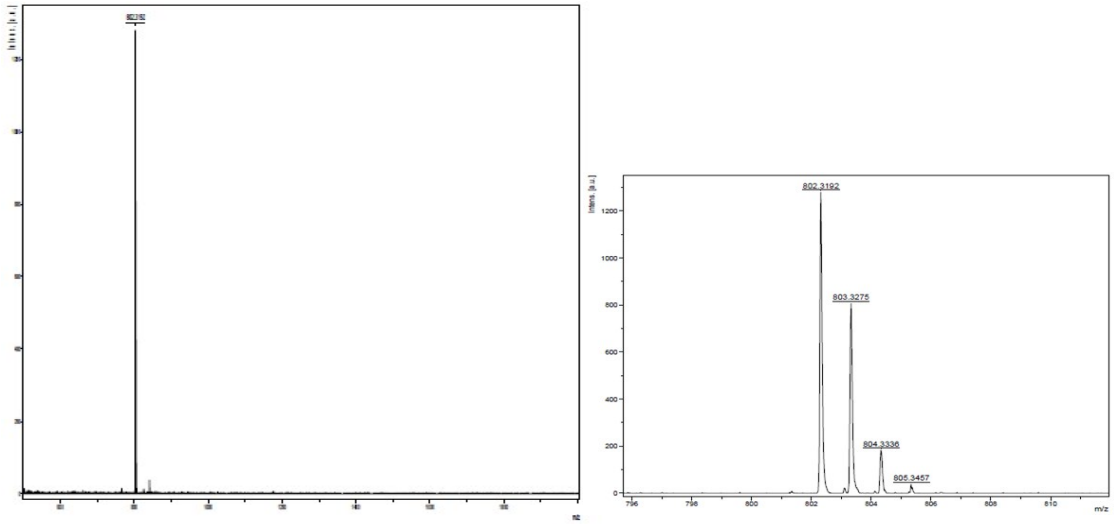

Figure S19 MALDI-HRMS (m/z) spectrum of **naft-3**.

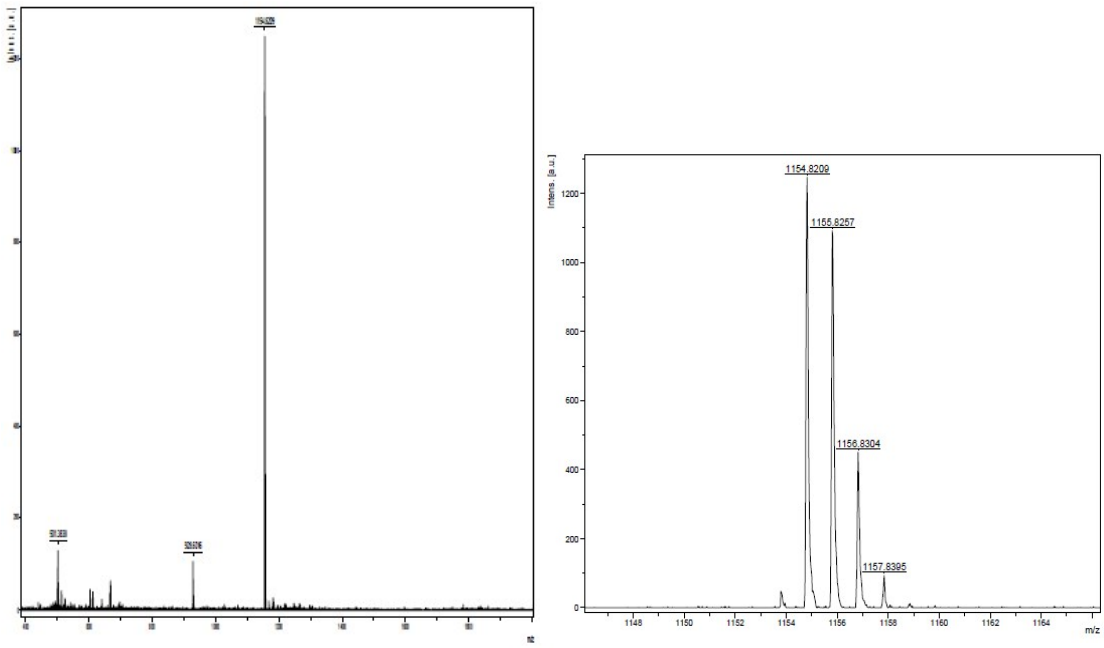

Figure S20 MALDI-HRMS (m/z) spectrum of **naft-4**.

3. UV-Vis and Electrochemical data

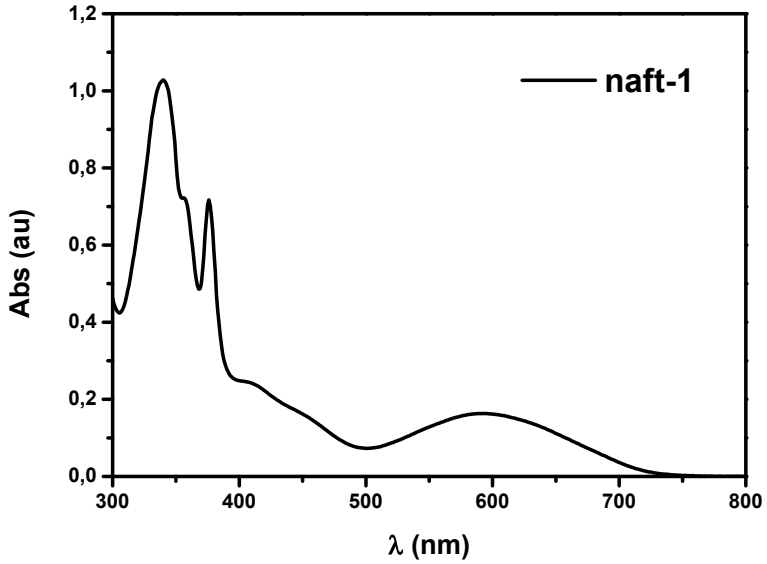

Figure S21 UV-Vis spectra of **naft-1** at 2.75x10^{-5} M in chloroform solution.

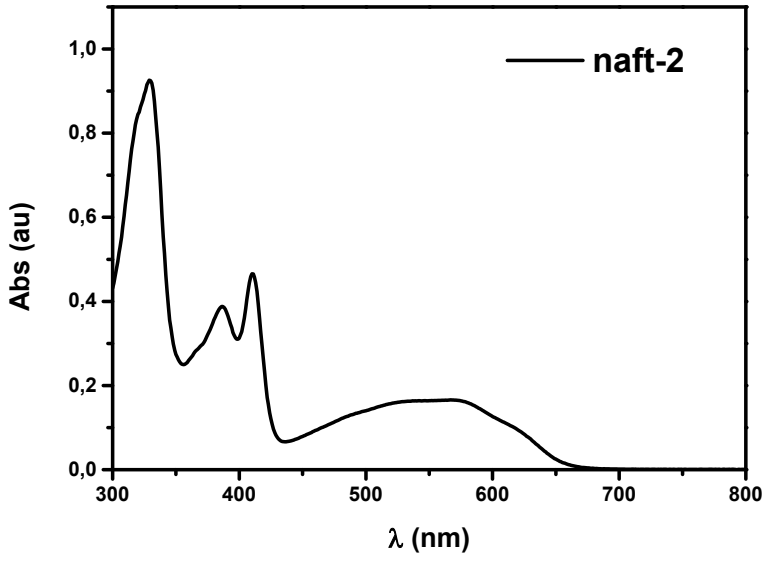

Figure S22 UV-Vis spectra of **naft-2** at 2.75x10^{-5} M in chloroform solution.

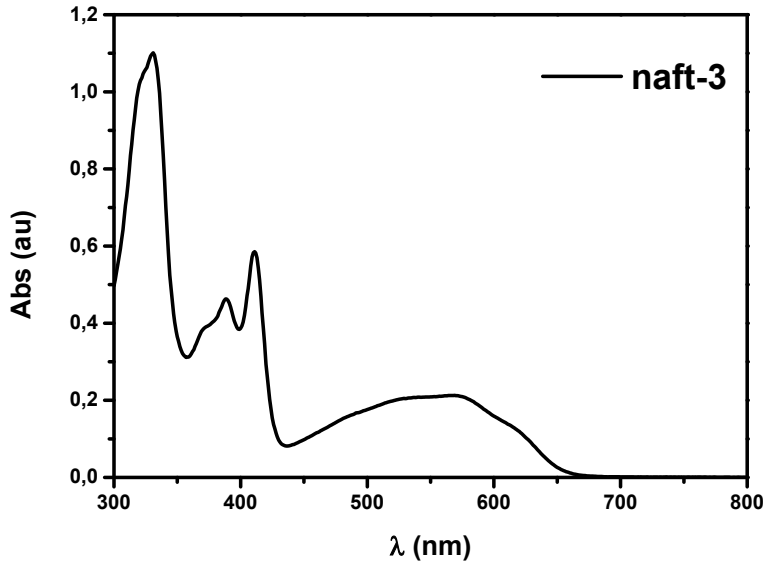

Figure S23 UV-Vis spectra of **naft-3** at 2.75x10^{-5} M in chloroform solution.

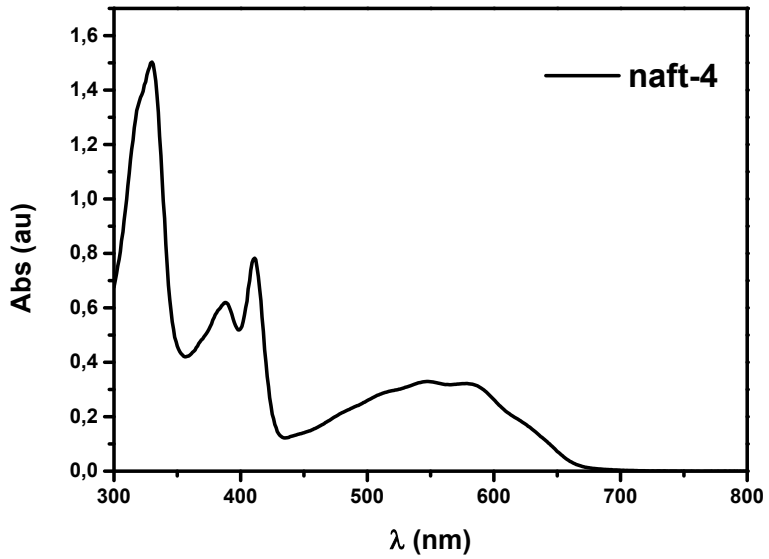

Figure S24 UV-Vis spectra of **naft-4** at 2.75x10^{-5} M in chloroform solution.

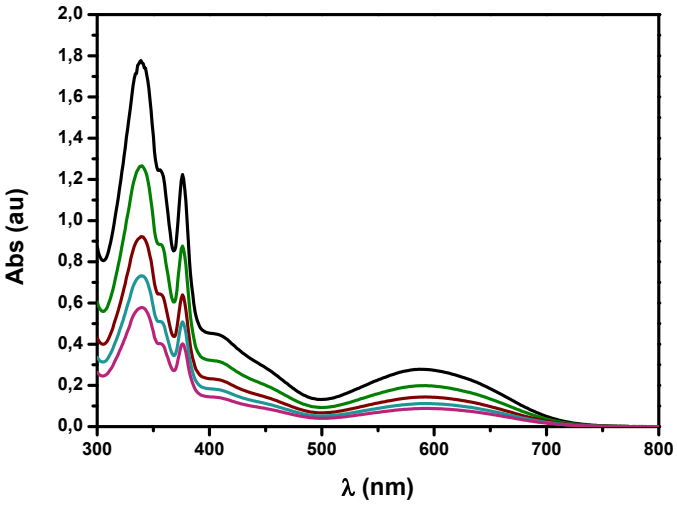

Figure S25 UV-Vis spectra of **naft-1** dilutions in chloroform solution.

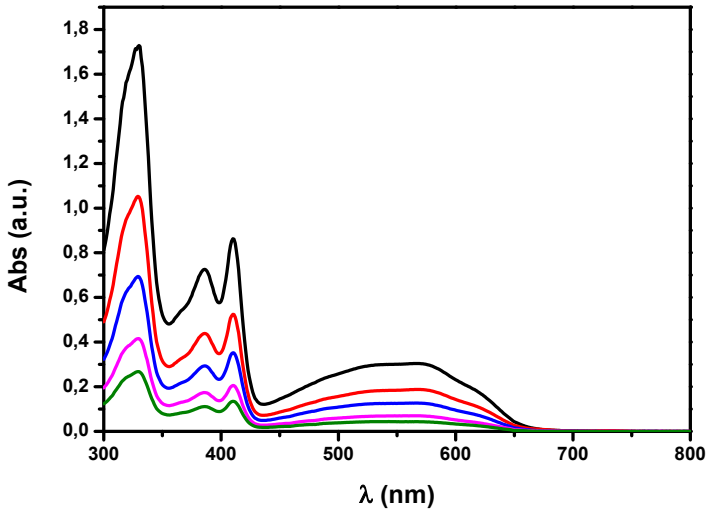

Figure S26 UV-Vis spectra of **naft-2** dilutions in chloroform.

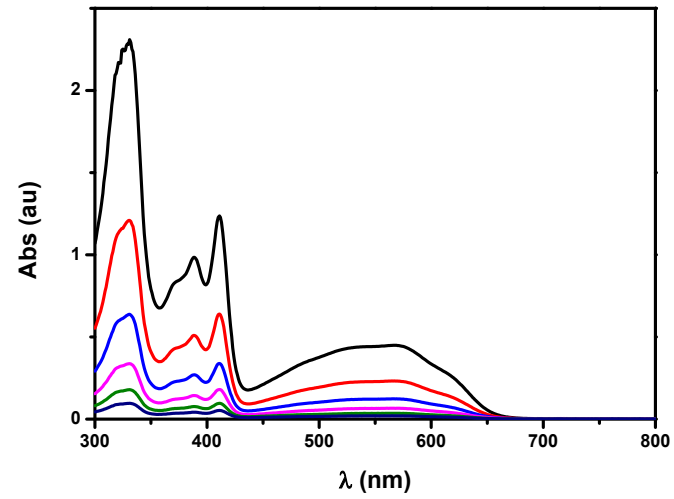

Figure S27 UV-Vis spectra of **naft-3** dilutions in chloroform solution.

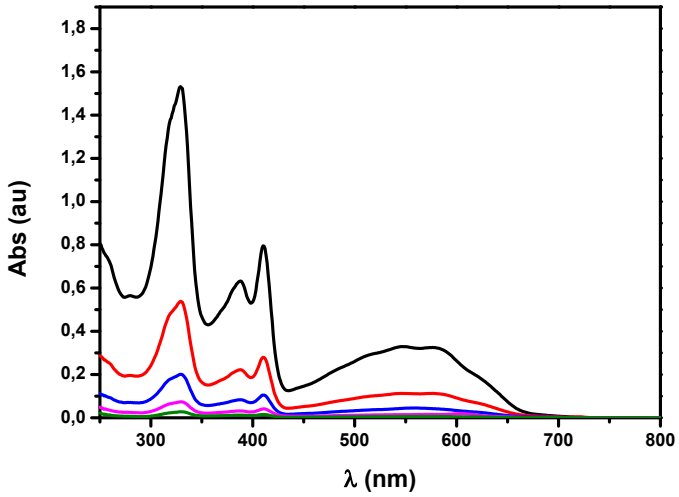

Figure S28 UV-Vis spectra of **naft-4** dilutions in chloroform solution.

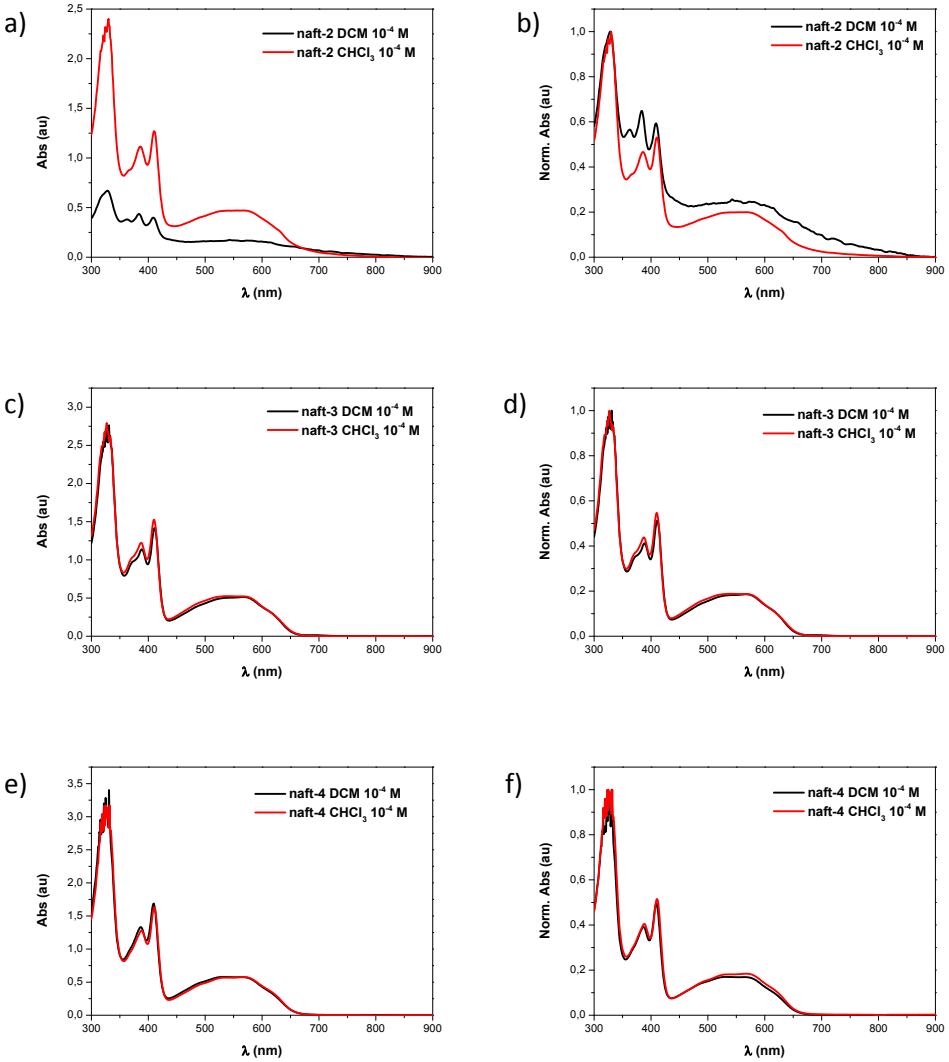

Figure S29 a),b) **naft-2**, c),d) **naft-3** and e),f) **naft-4** UV-vis comparison in different solvents at the same concentration.

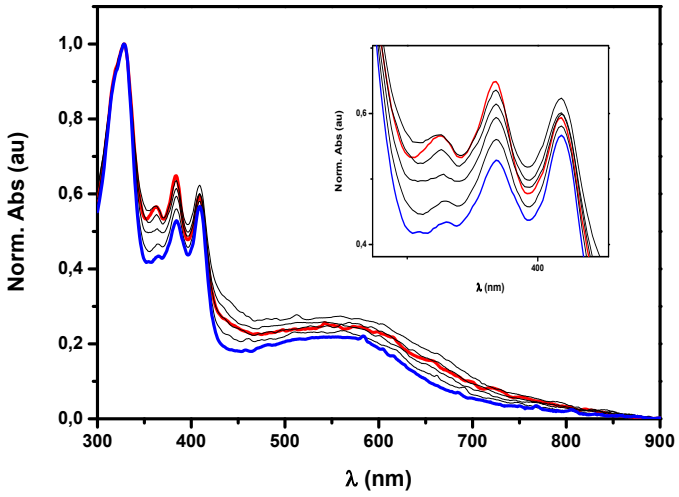

Figure S30 Dilution experiment for **naft-2** in dichloromethane.

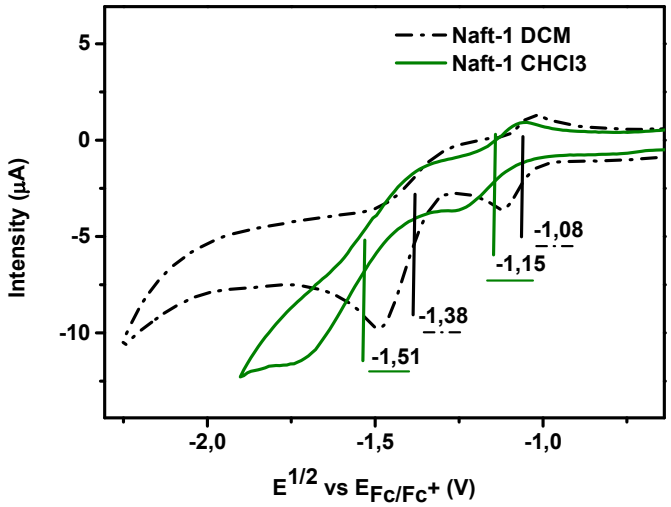

Figure S31 Cyclic voltammetry comparison for **naft-1** in dichloromethane and chloroform.

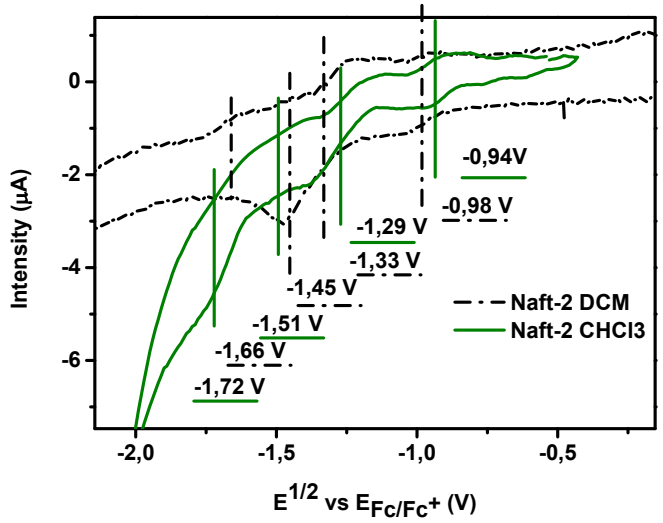

Figure S32 Cyclic voltammetry comparison for **naft-2** in dichloromethane and chloroform.

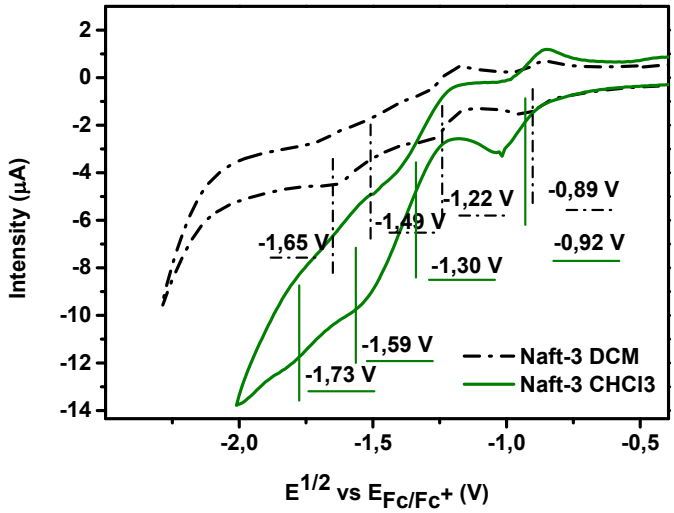

Figure S33 Cyclic voltammetry comparison for **naft-3** in dichloromethane and chloroform.

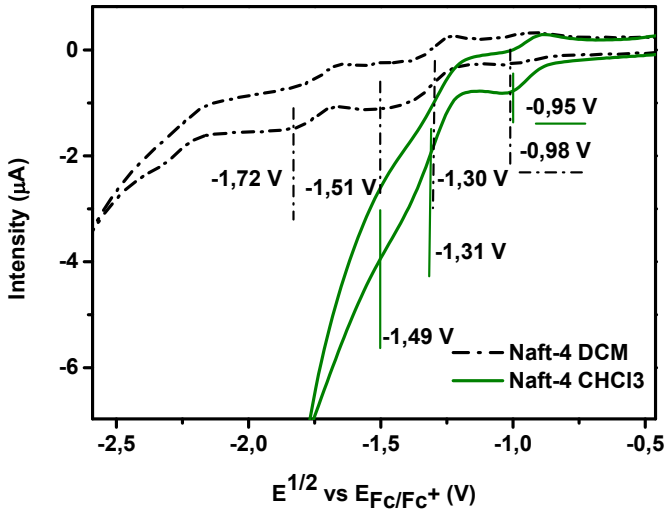

Figure S34 Cyclic voltammetry comparison for **naft-4** in dichloromethane and chloroform.

4. DFT Calculations

Theoretical calculations for the naft-1-4 dimers were carried out in the frame of density functional theory (DFT), using the B3LYP functional[4-6] and the 6-31G** basis set[7, 8] as implemented in the Gaussian 16 program.[9] The large alkyl chains on the N-imide group of **naft-1-2-4** were replaced with isopropyl and slightly larger chains to simplify the calculations. Geometry optimizations were performed without any symmetry constrains. On the basis of the resulting ground-state geometries, harmonic vibrational frequencies were calculated at the same theoretical level. The reorganization energies were calculated directly from the relevant points on the potential energy surfaces by using previously reported standard procedures. The PBE0 functional[10] was also use for a comparative purpose, however the results obtained are similar to those obtained with the B3LYP functional.

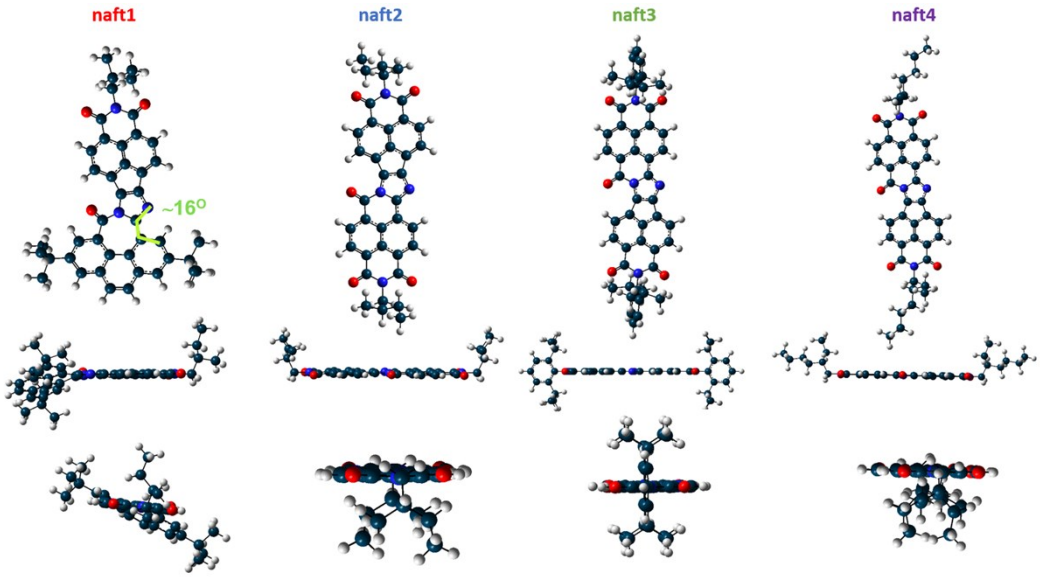

Figure S35 B3LYP/6-31G** optimized geometries of naft-1-4.

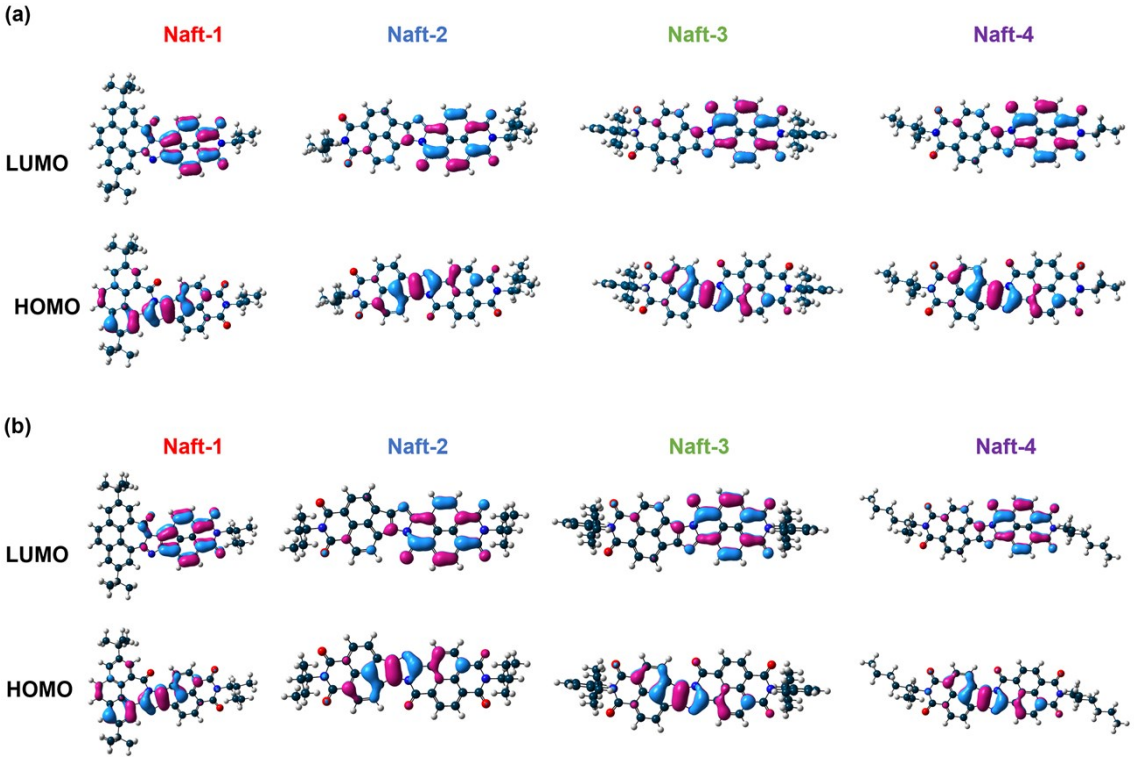

Figure S36 (a) B3LYP/6-31G** and (b) PBE0/6-31G** (PCM:DCM) frontier molecular orbital topologies predicted for naft-1-4.

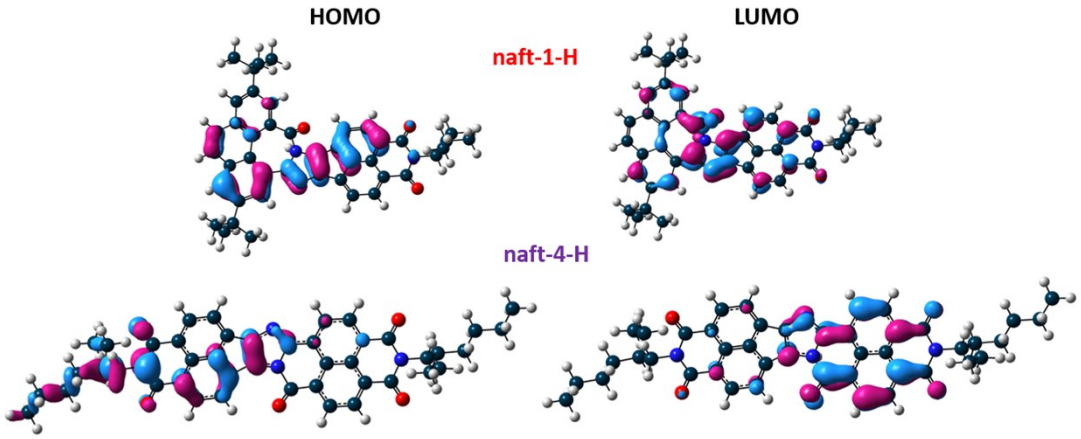

Figure S37 B3LYP/6-31G** frontier molecular orbital topologies predicted for naft-1 and naft-4 protonated tautomers.

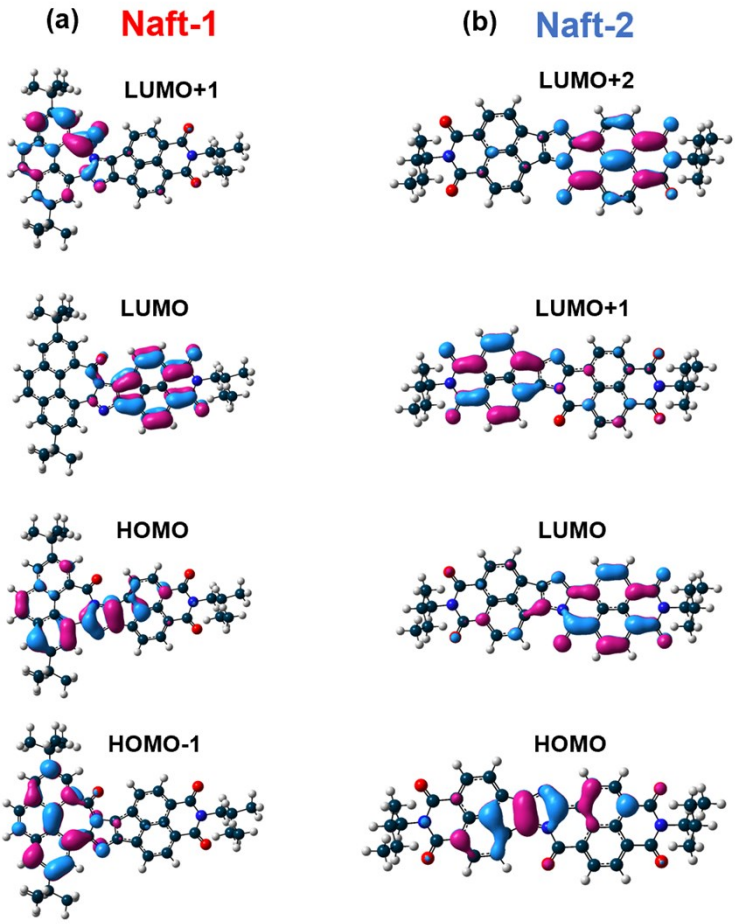

Figure S38 PBE0/6-31G** (PCM:DCM) molecular orbital topologies predicted for (a) naft-1 and (b) naft-2.

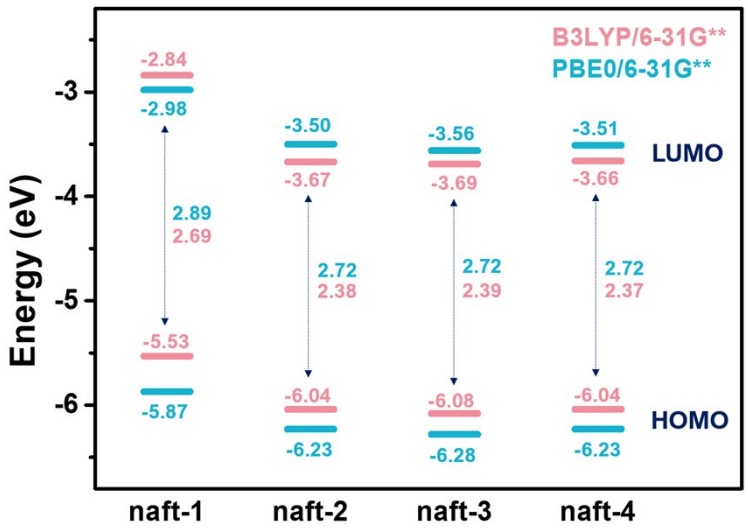

Figure S39 Frontier molecular orbital topologies predicted for naft-1-4 and the energy gap values with the B3LYP/6-31G** and PBE0/6-31G** (PCM:DCM) functionals.

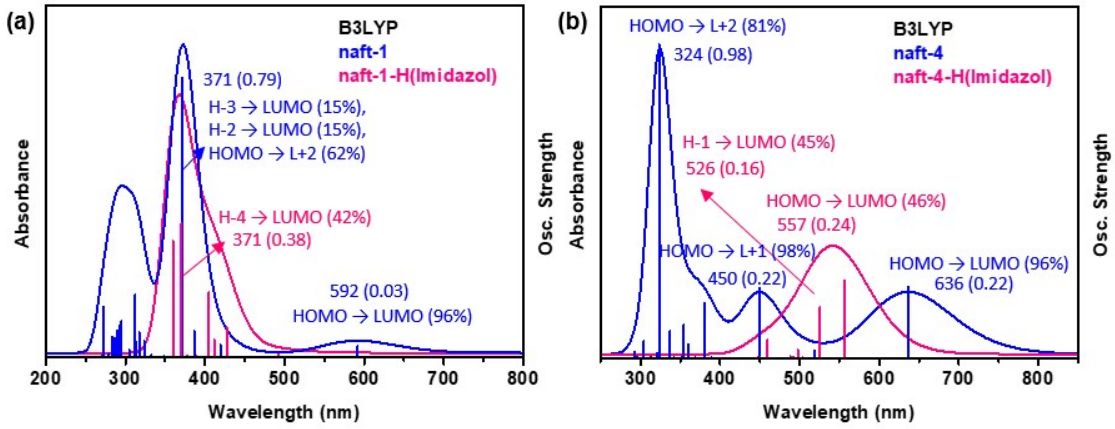

Figure S40 TDDFT/B3LYP-calculated vertical transition energies for (a) naft-1 and (b) naft-4 protonated species.

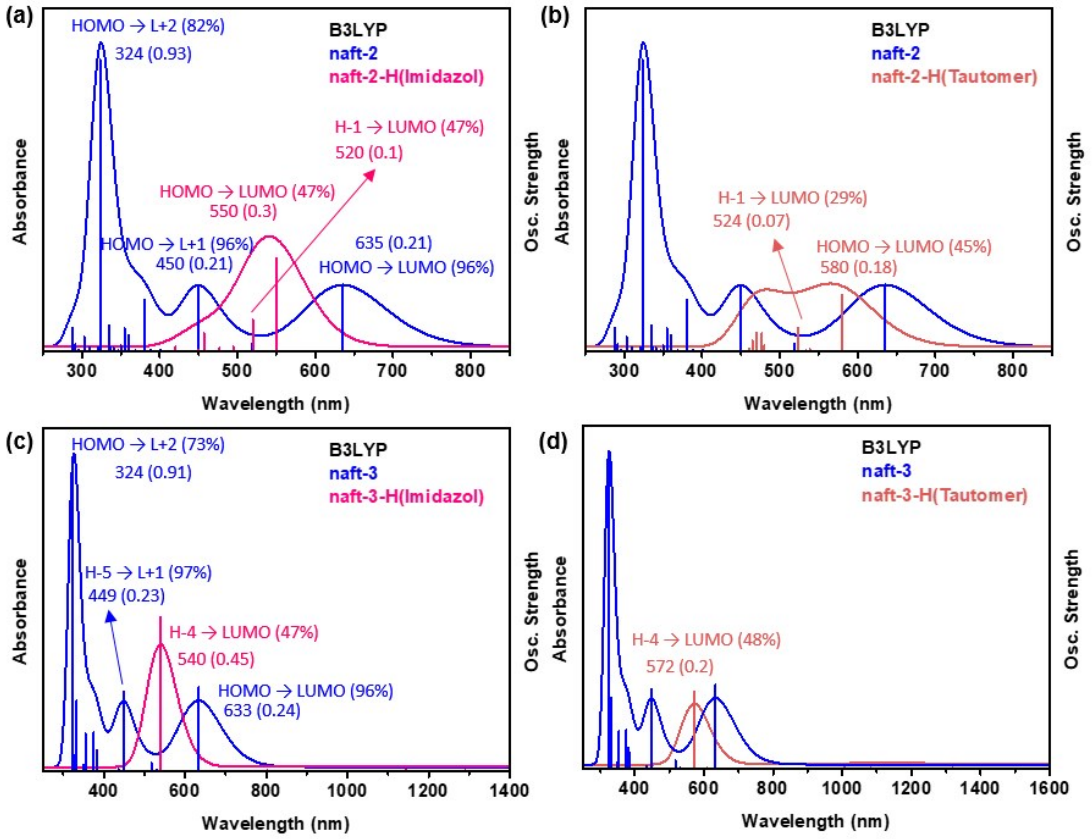

Figure S41 TDDFT/B3LYP-calculated vertical transition energies for different protonated species of (a-b) naft-2 and (b-c) naft-3.

Table S1. Calculated (PBE0/6-31G** (PCM:DCM) HOMO and LUMO energy levels, reorganization energies for **naft-1-4**. Experimental values are also shown.

	Experimental results			**Theoretical results**			**Reorganization energies**	
	LUMO (eV)	**HOMO (eV)**	**E_{gap} (eV)**	**LUMO (eV)**	**HOMO (eV)**	**E_{gap} (eV)**	**λ_e**	**λ_h**
naft-1	-4.02	-6.02	2	-2.79	-5.78	2.99	0.28	0.29
naft-2	-4.12	-6.01	1.89	-3.62	-6.30	2.68	0.21	0.30
naft-3	-4.21	-6.11	1.9	-3.65	-6.34	2.69	0.22	0.30
naft-4	-4.12	-6.01	1.89	-3.62	-6.30	2.68	0.22	0.30

Table S2. Optical characterization and TDDFT calculations at PBE0/6-31G** (PCM:DCM) level for **naft-1-4**.								
Molecules	λ_{exp} (nm)		λ_{theor} (nm)		**Description**		**f**	
	λ_{max} (nm)	λ_{ICT} (nm)	λ_{max} (nm)	λ_{ICT} (nm)	λ_{max} (nm)	λ_{ICT} (nm)	λ_{max} (nm)	λ_{ICT} (nm)
naft-1	335	587	362	587	HOMO→L+2	HOMO→LUMO	0.56	0.05
naft-2	328	551	310	600	HOMO→L+2	HOMO→LUMO	0.70	0.28
naft-3	329	551	315	601	HOMO→L+2	HOMO→LUMO	0.43	0.31
naft-4	328	551	310	602	HOMO→L+2	HOMO→LUMO	0.55	0.28

5. Spectroelectrochemical measurements

In-situ UV-Vis-NIR Spectroelectrochemical studies were conducted in dichloromethane and chloroform solutions (10^{-3}M) at room temperature by using 0.1M Bu_4NBF_4 as supporting electrolyte. The diluted solution was introduced in an optically transparent thin-layer electrochemical (OTTLE) cell from Specac, positioned in the sample compartment of a Varian Cary 5000 Spectrophotometer. The OTTLE cell consists of three electrodes: a Pt gauze used as the working electrode (32 wires per cm), a Pt wire used as the counter electrode, and an Ag wire used as the pseudo-reference electrode. This OTTLE is connected to an EC Epsilon potentiostat which controls a C3 epsilon potentiostat from BASi which provides the necessary voltage to reduce or oxidized the samples. The spectra were collected at constant potential electrolysis with an interval of 10 mV.

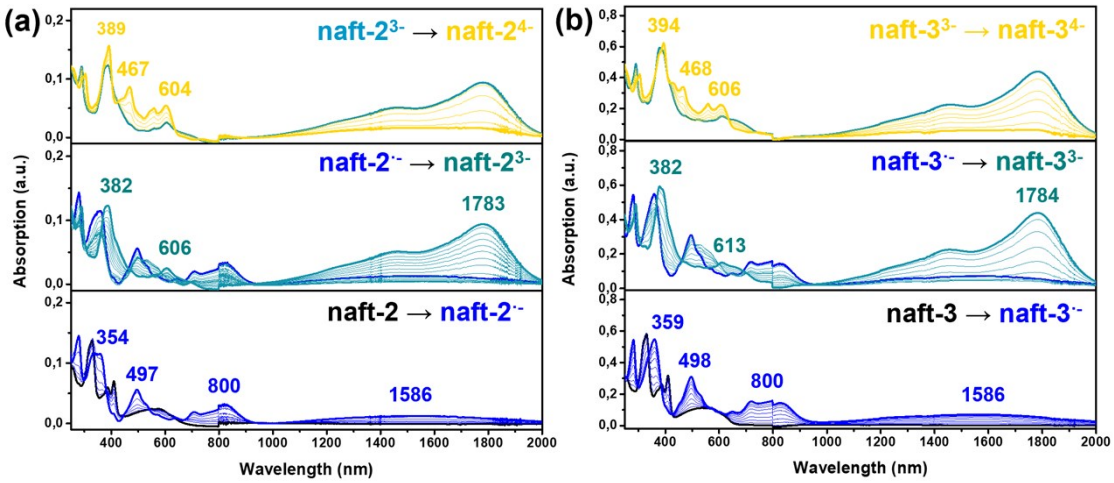

Figure S42 UV-Vis-NIR absorption spectra recorded during the first step of electrochemical reduction (-550/-490 V, blue curve), the second step of electrochemical reduction (-970/-710 V, cyan curve) and the third step of the electrochemical reduction (-1160/-1050 V, yellow curve) of (a) naft-2 and (b) naft-3 in dichloromethane in presence of Bu_4NBF_4 as supporting electrolyte within an OTTLE cell.

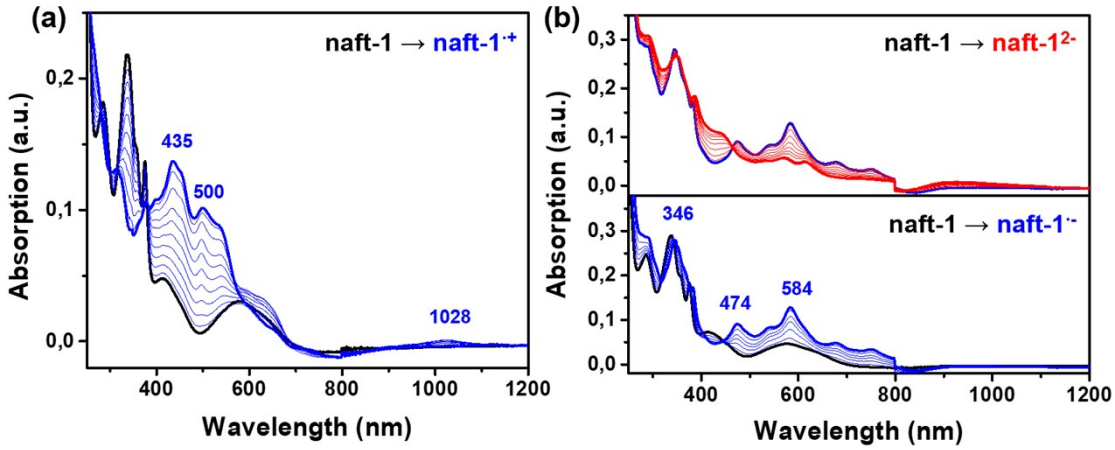

Figure S43 UV-Vis-NIR absorption spectra recorded by (a) electrochemical oxidation (1520 mV, blue curve), and (b) during the first step of electrochemical reduction (-790 mV, blue curve) and during the second step of the electrochemical reduction (-1040 mV, red curve) of naft-1 in chloroform in presence of Bu_4NBF_4 as supporting electrolyte within an OTTLE cell.

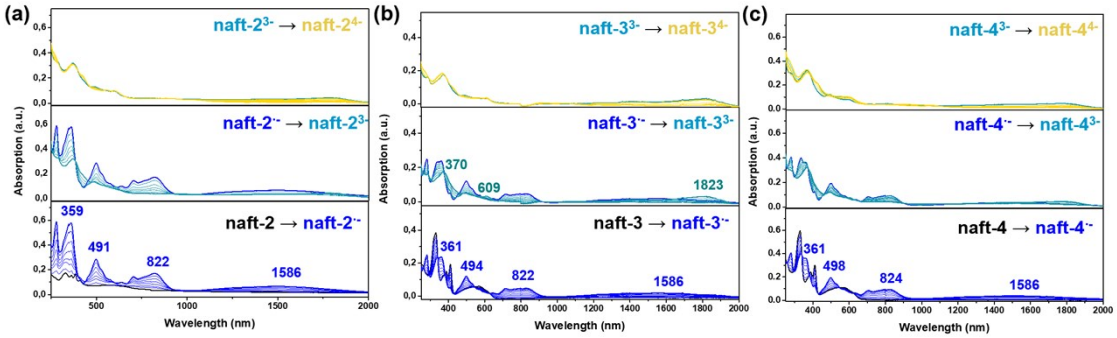

Figure S44 UV-Vis-NIR absorption spectra recorded during the first step of electrochemical reduction (-490 V, blue curve), the second step of electrochemical reduction (-720 V, cyan curve) and the third step of the electrochemical reduction (1070 V, yellow curve) of (a) naft-2 (b) naft-3 and (c) naft-4 in chloroform in presence of Bu_4NBF_4 as supporting electrolyte within an OTTLE cell.

Table S3. Relative energies difference between PBE0/6-31G**- PCM:DCM and PCM:CF for naft-1-2.							
	Theoretical results						
	Solvent	Neutral	Cation	Anion	Dianion	Trianion	Tetraanion
naft-1	PCM:DCM	0	0	0	0	-	-
	PCM:CF	1.28	3.90	5.30	15.49	-	-
naft-2	PCM:DCM	0	-	0	0	0	0
	PCM:CF	1.41	-	4.07	12.34	26.17	45.48

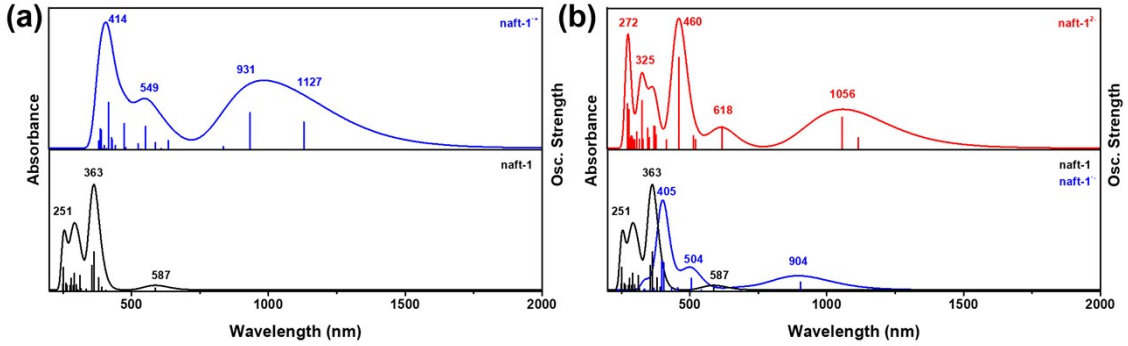

Figure S45 TDDFT/PBE0 (PCM:DCM)-calculated vertical transition energies for naft-1 (a) oxidized species and (b) reduced species.

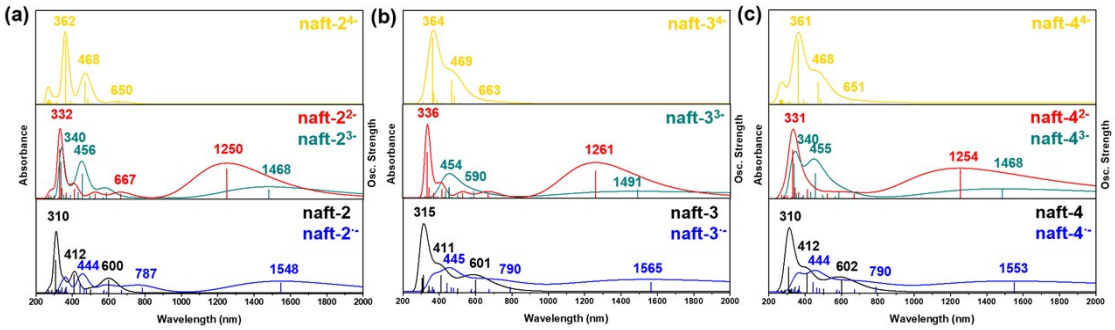

Figure S46 TDDFT/PBE0 PCM(DCM)-calculated vertical transition energies for (a) naft-2, (b) naft-3 and (c) naft-4 with the different reduced species.

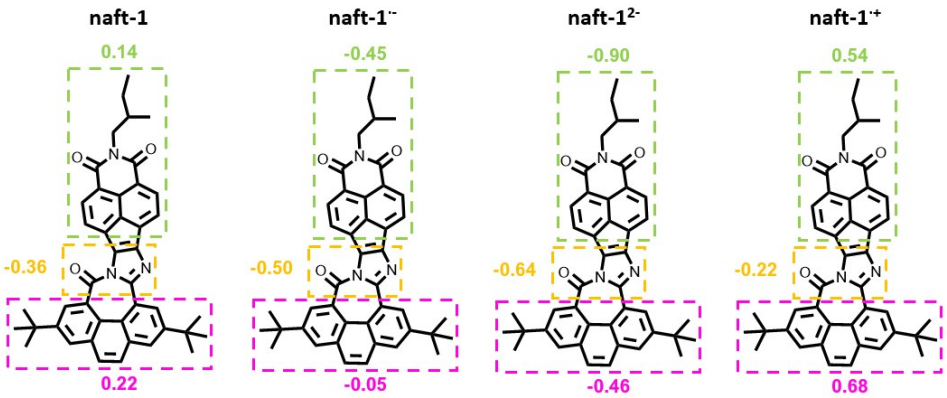

Figure S47 B3LYP/6-31G**-charge distributions for naft-1 as neutral, anion, dianion and cation species.

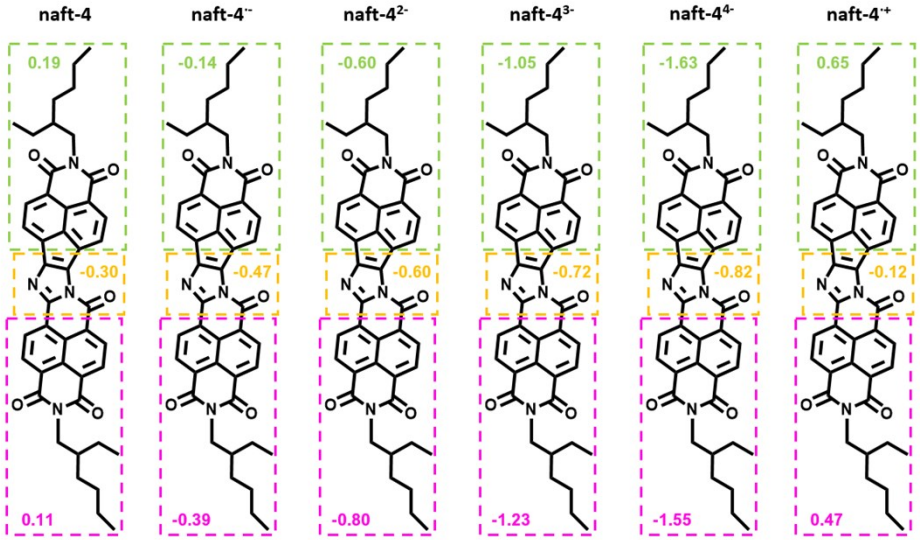

Figure S48 B3LYP/6-31G**-charge distributions for naft-4 as neutral, anion, dianion, trianion, tetraanion and cation species.

6. OFET fabrication details

Bottom-gate top-contact OTFTs were fabricated using the studied molecules as the active layer. Gate dielectrics (d-doped Si wafers with 300 nm thermally grown SiO_2 dielectric layers) were functionalized with octadecyltrichlorosilane (OTS) self-assembled monolayer. The capacitance of the 300 nm SiO_2 gate insulator was 10 $nFcm^{-2}$. Prior to the surface functionalization, the wavers were solvent cleaned by immersing them twice for 30 s each in EtOH with sonication, drying with a stream of N_2, and treating with UV-ozone for 10 min. the cleaned silicon wafers were treated with OTS by immersion in a 3.0 mM humidity-exposed OTS-hexane solution for 1 h, as previously described (Ref). Following OTS deposition, the substrates were sonicated with hexane, acetone, and

ethanol, and dried with a N_2 stream. Next, the semiconductors were vapor-deposited on substrates at either room temperature or preheated at 90ºC. The deposition rate was oscillating between 0.06-0.2 Å/s at a vacuum of $4{,}1x10^{-6}$ mbar. OFET devices were completed by gold vapor deposition through a shadow mask to define devices with various channel lengths and channel widths. The devices were characterized under vacuum conditions in an EB-4 Everbeing probe station with a 4200-SCS/C Keithley semiconductor characterization system.

7. Atomic Force Microscopy

Atomic Force Microscopy (AFM) measurements were conducted using a diMultiMode™V Atomic Force Microscope from Veeco Instruments-Nanoscope V in the tapping mode. AFM measurements were carried out at the Research Central Services (SCAI) of the University of Málaga.

Table S4. AFM measured surface roughness of the thin films of naft molecules.

Molecules	RMS (nm)
naft-1	5.0
naft-2	3.4
naft-3	0.9
naft-4	15.6

8. REFERENCES

1. P. de Echegaray, M. J. Mancheño, I. Arrechea-Marcos, R. Juárez, G. López-Espejo, J. T. López Navarrete, M. M. Ramos, C. Seoane, R. P. Ortiz and J. L. Segura, *J. Org. Chem.*, 2016, **81**, 11256-11267.
2. H. Herrera, P. de Echegaray, M. Urdanpilleta, M. J. Mancheño, E. Mena-Osteritz, P. Bäuerle and J. L. Segura, *Chem. Commun.*, 2013, **49**, 713-715.
3. H. Li, F. S. Kim, G. Ren, E. C. Hollenbeck, S. Subramaniyan and S. A. Jenekhe, *Angew. Chem. Int. Ed.*, 2013, **52**, 5513-5517.
4. A. D. Becke, *J. Chem. Phys.*, 1993, **98**, 1372-1377.
5. A. D. Becke, *J. Chem. Phys.*, 1993, **98**, 5648-5652.
6. C. Lee, W. Yang and R. G. Parr, *Phys. Rev. B Condens. Matter*, 1988, **37**, 785-789.
7. P. C. Hariharan and J. A. Pople, *Theoret. Chim. Acta*, 1973, **28**, 213-222.
8. W. J. Hehre and W. A. Lathan, *J. Chem. Phys.*, 1972, **56**, 5255-5257.
9. G. W. S. M. J. T. Frisch, H. B.; Scuseria, G. E.; Robb, M. A.; Cheeseman, J. R.; Scalmani, G.; Barone, V.; Petersson, G. A.; Nakatsuji, H.; Li, X.; Caricato, M.; Marenich, A. V.; Bloino, J.; Janesko, B. G.; Gomperts, R.; Mennucci, B.; Hratchian, H. P.; Ortiz, J. V.; Izmaylov, A. F.; Sonnenberg, J. L.; Williams-Young, D.; Ding, F.; Lipparini, F.; Egidi, F.; Goings, J.; Peng, B.; Petrone, A.; Henderson, T.; Ranasinghe, D.; Zakrzewski, V. G.; Gao, J.; Rega, N.; Zheng, G.; Liang, W.; Hada, M.; Ehara, M.; Toyota, K.; Fukuda, R.; Hasegawa, J.; Ishida, M.; Nakajima, T.; Honda, Y.; Kitao, O.; Nakai, H.; Vreven, T.; Throssell, K.; Montgomery, J. A., Jr.; Peralta, J. E.; Ogliaro, F.; Bearpark, M. J.; Heyd, J.

J.; Brothers, E. N.; Kudin, K. N.; Staroverov, V. N.; Keith, T. A.; Kobayashi, R.; Normand, J.; Raghavachari, K.; Rendell, A. P.; Burant, J. C.; Iyengar, S. S.; Tomasi, J.; Cossi, M.; Millam, J. M.; Klene, M.; Adamo, C.; Cammi, R.; Ochterski, J. W.; Martin, R. L.; Morokuma, K.; Farkas, O.; Foresman, J. B.; Fox, D. J. Gaussian, Inc., Wallingford CT., 2016.

10. T. Körzdörfer and J.-L. Brédas, *Accounts of Chemical Research*, 2014, **47**, 3284-3291.